Comparison of aAqueous SOA product distributions formation from photosensitized guaiacol oxidation by: Comparison between non-phenolic and phenolic methoxybenzaldehydes as photosensitizers in the absence and presence of ammonium nitrate

Beatrix Rosette Go Mabato[1,2], Yong Jie Li[3], Dan Dan Huang[4], Yalin Wang[3], and Chak K. Chan[1,2]*

[1]School of Energy and Environment, City University of Hong Kong, Hong Kong, China
[2]City University of Hong Kong Shenzhen Research Institute, Shenzhen, China
[3]Department of Civil and Environmental Engineering, and Centre for Regional Ocean, Faculty of Science and Technology, University of Macau, Macau, China
[4]Shanghai Academy of Environmental Sciences, Shanghai 200233, China

Correspondence to: Chak K. Chan (Chak.K.Chan@cityu.edu.hk)

Abstract. Aromatic carbonyls (e.g., methoxybenzaldehydes), an important class of photosensitizers, are abundant in the atmosphere. Photosensitization and nitrate-mediated photo-oxidation can occur simultaneously, yet studies about their interactions, particularly for aqueous secondary organic aerosol (aqSOA) formation, remain limited. This study compared non-phenolic (3,4-dimethoxybenzaldehyde, DMB) and phenolic (vanillin, VL) methoxybenzaldehydes as photosensitizers for aqueous secondary organic aerosol (aqSOA) formation via guaiacol (GUA) oxidation in the absence and presence of ammonium nitrate (AN) under atmospherically relevant cloud and fog conditions. The effects of ammonium nitrate (AN) on these reactions were also explored. GUA oxidation by triplet excited states of DMB (^{3}DMB*) (GUA+DMB) was ~4 times faster and exhibited greater light absorption than oxidation by ^{3}VL* (GUA+VL). Both GUA+DMB and GUA+VL formed aqSOA composed of oligomers, functionalized monomers, oxygenated ring-opening species, and N-containing products in the presence of AN. The observation of N-heterocycles such as imidazoles indicates the participation of ammonium in the reactions. The majority of generated aqSOA are potential brown carbon (BrC) chromophores. Oligomerization and functionalization dominated in GUA+DMB and GUA+VL, but functionalization appeared to be more important in GUA+VL due to contributions from VL itself. AN did not significantly affect the oxidation kinetics, but it had distinct effects on the product distributions, likely due to differences in the photosensitizing abilities and structural features of DMB and VL. In particular, the more extensive fragmentation in GUA+DMB than in GUA+VL likely generated more N-containing products in GUA+DMB+AN. In GUA+VL+AN, the increased oligomers may be due to VL-derived phenoxy radicals induced by $^\cdot$OH or $^\cdot$NO$_2$ from nitrate photolysis. Furthermore, increased nitrated products observed in the presence of both DMB or VL and AN than in AN alone implies that photosensitized reactions may promote nitration. This work demonstrates how the structural features of photosensitizers affect aqSOA formation via non-carbonyl phenol oxidation.

32 Potential interactions between photosensitization and AN photolysis were also elucidated. These findings facilitate a better

33 understanding of photosensitized aqSOA formation and highlight the importance of ~~ammonium nitrate~~AN photolysis in

34 these reactions.

1 Introduction

36 Photosensitized reactions involving triplet excited states of organic compounds ($^3C^*$) are efficient pathways for the

37 formation of secondary organic aerosol in the aqueous phase (aqSOA; Smith et al., 2014, 2016; Yu et al., 2014, 2016; Chen

38 et al., 2020; Jiang et al., 2021; Misovich et al., 2021; Mabato et al., 2022). Upon irradiation by solar radiation,

39 photosensitizers form an excited triplet state that directly reacts with substrates (e.g., phenols), and can generate singlet

40 oxygen ($^1O_2$), superoxide ($O_2^{\bullet-}$) or hydroperoxyl ($^{\bullet}HO_2$) radicals, and hydroxyl radicals ($^{\bullet}OH$) upon reactions with O_2 and

41 substrates (George et al., 2018; Chen et al., 2020), thereby facilitating the oxidation of rather volatile species and

42 contributing to aqSOA formation. An important class of photosensitizers is aromatic carbonyls (e.g.,

43 methoxybenzaldehydes) which are abundant in aerosol particles, cloud waters, and fog waters (Anastasio et al., 1997; Felber

44 et al., 2021). Aromatic carbonyls can be emitted from anthropogenic sources and biomass burning (BB; Lipari et al.,1984;

45 Edye and Richards, 1991; Hawthorne et al., 1992; Simoneit et al., 1993, 1999; Anastasio et al., 1997; Felber et al., 2021), or

46 formed via atmospheric oxidation of aromatic hydrocarbons (Hoshino et al., 1978; Calvert and Madronich, 1987; Anastasio

47 et al., 1997; Felber et al., 2021). BB is also a significant source of phenols through lignin pyrolysis (Simpson et al., 2005).

48 Phenolic carbonyls have a hydroxyl (–OH) group on the aromatic ring, whereas non-phenolic carbonyls do not. BB smoke

49 has been reported to have comparable concentrations of phenolic and non-phenolic carbonyls (Simoneit et al., 1993;

50 Anastasio et al., 1997).

51   Most previous studies on aqSOA formation via photosensitized non-carbonyl phenol oxidation have examined 3,4-

52 dimethoxybenzaldehyde (DMB), a non-phenolic methoxybenzaldehyde, as the photosensitizer (Smith et al., 2014, 2015; Yu

53 et al., 2014, 2016; Chen et al., 2020; Jiang et al., 2021; Misovich et al., 2021). By contrast, phenolic carbonyls have been

54 mainly studied as aqSOA precursors via $^{\bullet}OH$-, nitrate-, nitrite-, and $^3DMB^*$-mediated oxidation (Li et al., 2014; Huang et al.,

55 2018; Pang et al., 2019; Jiang et al., 2021; Misovich et al., 2021). However, strongly light-absorbing phenolic carbonyls

56 (e.g., molar absorptivity above 300 nm $\geq 7 \times 10^3$ M^{-1} cm^{-1}) can also serve as photosensitizers to promote aqSOA formation

57 (Smith et al., 2016; Mabato et al., 2022). For instance, the direct photosensitized oxidation of phenolic carbonyls (i.e.,

58 oxidation of phenolic carbonyls by their $^3C^*$ or $^3C^*$-derived oxidants) such as vanillin (VL; another methoxybenzaldehyde)

59 efficiently form low-volatility products, with aqSOA mass yields of up to 140% (Smith et al., 2016). Moreover, the aqSOA

60 mass yields from the oxidation of syringol by $^3DMB^*$ and $^3VL^*$ are similar (111% and 114%, respectively; Smith et al.,

61 2014, 2016). In addition, we recently reported that the direct photosensitized oxidation of VL and guaiacol oxidation by

62 $^3VL^*$ yield similar products (oligomers, functionalized monomers, and oxygenated ring-opening products) as observed with

63 $^3DMB^*$ (Yu et al., 2014; Mabato et al., 2022). Guaiacol is a non-carbonyl BB methoxyphenol with an emission rate from

64 fireplace wood combustion in the range of 172 to 279 mg/kg (Schauer et al., 2001; Simoneit, 2002). The atmospheric

65 reactivity of methoxyphenols has recently been reviewed (Liu et al., 2022). However, our previous experiments (Mabato et

66 al., 2022) were performed at a concentration (0.1 mM VL) higher than what was typically used for DMB (0.005 to 0.01 mM;

67 Smith et al., 2014, 2015; Yu et al., 2014, 2016). Therefore, direct comparisons between photosensitization by ^{3}DMB* and

68 ^{3}VL* cannot be made. Despite the above findings, much is still unknown about how aqSOA formation proceeds in systems

69 using phenolic carbonyls as photosensitizers.

70   BB aerosols are typically internally mixed with other aerosol components, such as ammonium nitrate (AN;

71 Zielinski et al., 2020). Hence, aromatic carbonyls and phenols may coexist with AN in BB aerosols. Nitrate and ammonium

72 facilitate the formation of aqSOA and brown carbon (BrC) via a number of pathways. Nitrate photolysis can produce $^•$OH

73 and nitrating agents (e.g., $^•$NO$_2$; Minero et al., 2007; Huang et al., 2018; Mabato et al., 2022; Wang et al., 2022; Yang et al.,

74 2022), and ammonium reacts with carbonyls to yield N-containing heterocycles (e.g., imidazoles) and oligomers capable of

75 UV-Vis light absorption (De Haan et al., 2009, 2011; Nozière et al., 2009, 2010, 2018; Shapiro et al., 2009; Yu et al., 2011;

76 Lee et al., 2013; Powelson et al., 2014; Gen et al., 2018; Grace et al., 2019; Mabato et al., 2019). Furthermore, nitrate

77 photolysis may be an important process for SO$_2$ oxidation and SOA formation in the particle phase (Gen et al., 2019a,

78 2019b, 2022; Zhang et al., 2020, 2021, 2022), and it can potentially modify the morphology of atmospheric viscous particles

79 (Liang et al., 2021). Yet, understanding of the effects of inorganic nitrate on aqSOA formation remains limited. In addition,

80 aqSOA formation studies involving aromatic carbonyls and phenols have probed either photosensitization or nitrate-

81 mediated photo-oxidation, but these reactions can occur simultaneously. For instance, we previously reported nitrated

82 compounds, including a potential imidazole derivative from the direct photosensitized oxidation of VL in the presence of AN

83 (Mabato et al., 2022). Accordingly, investigations on reaction systems including both photosensitizers and AN may provide

84 further insights into the aqueous-phase processing of BB aerosols.

85   In this work, we compared aqSOA formation from photosensitized guaiacol (GUA) oxidation by ^{3}C* of non-

86 phenolic and phenolic methoxybenzaldehydes under identical conditions (simulated sunlight and concentration) relevant to

87 cloud and fog waters. The effects of AN on photosensitized aqSOA formation were also examined. In this study, the

88 dominant aqSOA precursor is GUA (Henry's law constant of 9.2×10^2 M atm^{-1}; Sagebiel et al., 1992), and DMB and VL

89 were used as photosensitizers to oxidize GUA. DMB and VL (Henry's law constants of $\sim$5.4$7.3 \times 10^{\cancel{13}}$ M atm^{-1} and 4.7×10^5

90 M atm^{-1}, respectively; Yaws, 1994; EPI Suite version 4.1, 2012; Felber et al., 2021), which are also abundant in BB

91 emissions (Schauer et al., 2001; Li et al., 2014; Chen et al., 2017; Pang et al., 2019; Mabato et al., 2022) and whose

92 structures differ only by one functional group (–OCH$_3$ for the former and –OH for the latter, Fig. 1), represented non-

93 phenolic and phenolic methoxybenzaldehydes, respectively. The structures of GUA, DMB, and VL are provided in Figure 1.

94 Based on their quantum yield of ^{3}C* formation, DMB and VL have been classified as moderate and poor photosensitizers,

95 respectively (Felber et al., 2021). The photosensitized oxidation of GUA by ^{3}DMB* or ^{3}VL* in the absence (and presence)

96 of AN are referred to as GUA+DMB(+AN) and GUA+VL(+AN), respectively. GUA photo-oxidation by AN alone

97 (GUA+AN) was also explored for comparison with GUA+DMB+AN and GUA+VL+AN. The molar absorptivities of GUA,

98   DMB, VL, and nitrate are shown in Figure 1. The precursor and photosensitizer decay kinetics, detected products, and

99   absorbance enhancement were used to characterize the reactions. However, it should be noted that we mainly focused on the

100   analyses of the reaction products and product distribution.

101   While several studies on photo-oxidation of BB emissions are available, this work focuses on the comparison

102   between non-phenolic and phenolic methoxybenzaldehydes as photosensitizers in the absence and presence of AN for

103   aqSOA formation. We found that GUA oxidation by ^{3}DMB* was faster and exhibited greater light absorption relative to

104   GUA+VL. These are likely attributed to the stronger photosensitizing ability of DMB and the –OH group of VL, making it

105   more prone to oxidation and more reactive towards electrophilic aromatic substitution. Oligomerization and functionalization

106   dominated in GUA+DMB and GUA+VL, but functionalization appeared to be more significant in GUA+VL due to VL

107   transformation products. Although AN did not significantly influence the oxidation kinetics due to the predominant role of

108   photosensitizer chemistry compared to nitrate, AN promoted the formation of N-containing products. These include N-

109   heterocycles (e.g., imidazoles), suggesting the participation of ammonium in the reactions. Moreover, the product

110   distributions indicate distinct interactions between photosensitization by ^{3}DMB* and ^{3}VL* and AN photolysis. In particular,

111   AN generated more N-containing products in GUA+DMB+AN than in GUA+VL+AN, and increased the oligomers in

112   GUA+VL+AN. Furthermore, increased nitrated compounds in GUA+DMB+AN and GUA+VL+AN compared to GUA+AN

113   suggest that photosensitized reactions may promote reactions by nitrate photolysis.

114   **2 Methods**

115   **2.1 Aqueous phase photo-oxidation experiments**

116   Procedures for the photo-oxidation experiments are presented in detail in our previous study (Mabato et al., 2022).

117   Experimental solutions were prepared using 0.1 mM guaiacol (GUA, Sigma Aldrich, ≥98.0%) and 0.01 mM 3,4-

118   dimethoxybenzaldehyde (DMB, Acros Organics, 99+%) or 0.01 mM vanillin (VL, Acros Organics, 99%, pure), in the

119   absence and presence of ammonium nitrate (1 mM; AN, Acros Organics, 99+%, for analysis). These GUA and

120   methoxybenzaldehydes concentrations are within the values expected in cloud or fog drops in areas with significant wood

121   combustion (Anastasio et al., 1997; Rogge et al., 1998; Nolte et al., 2001). The AN concentration represents values usually

122   observed in cloud and fog waters (Munger et al., 1983; Collett et al., 1998; Zhang and Anastasio, 2003; Li et al., 2011;

123   Giulianelli et al., 2014; Bianco et al., 2020). It must be noted that this study did not intend to identify the AN concentrations

124   that would affect the kinetics but attempted to analyze the effects of AN on photosensitized aqSOA formation. A solution

125   composed of 0.1 mM GUA and 1 mM AN (GUA+AN) was also examined for comparison with GUA+DMB+AN and

126   GUA+VL+AN. Sulfuric acid (H_2SO_4; Acros Organics, ACS reagent, 95% solution in water) was used to adjust the pH of the

127   solutions to 4, which is within typical cloud pH values (2–7; Pye et al., 2020) and pH values observed in wood burning-

128   impacted cloud and fog waters (Collett et al., 1998; Raja et al., 2008). The solutions (initial volume of 500 mL) were

129   bubbled with synthetic air (0.5 dm^3/min) for 30 min before irradiation and throughout the reactions to achieve air-saturated

130 conditions (Du et al., 2011; Chen et al., 2020) and were continuously magnetically stirred. In this study, the reactions can

131 generate ^{3}DMB*/^{3}VL* and secondary oxidants ($^1O_2$, $O_2^{\cdot-}$/$^{\cdot}HO_2$, $^{\cdot}OH$) but not ozone. Solutions contained in a quartz

132 photoreactor were irradiated using a xenon lamp (model 6258, Ozone free xenon lamp, 300 W, Newport) equipped with a

133 longpass filter (20CGA-305 nm cut-on filter, Newport) to eliminate light below 300 nm. The reaction temperatures were

134 maintained at 27 ± 2 °C using cooling fans positioned around the photoreactor and lamp housing. The averaged initial

135 photon flux in the reactor measured from 300 to 380 nm was ~3×10^{15} photons cm^{-2} s^{-1} nm^{-1} (Fig. 1), similar to our previous

136 work (Mabato et al., 2022). Samples were collected every 30 mins for 180 mins for offline analyses of (1) GUA, DMB, and

137 VL concentrations using ultra-high-performance liquid chromatography with photodiode array detector (UHPLC-PDA) ; and

138 (2) absorbance measurements using UV-Vis spectrophotometry. Moreover, the samples collected before and after irradiation

139 (180 min) were analyzed for (32) reaction products using UHPLC coupled with heated electrospray ionization Orbitrap mass

140 spectrometry (UHPLC-HESI-Orbitrap-MS) operated in positive and negative ion modes and; (43) concentrations of small

141 organic acids using ion chromatography (IC).; and (4) absorbance measurements using UV-Vis spectrophotometry. Each

142 experiment was repeated independently at least three times. The reported decay rate constants, small organic acids

143 concentration, and absorbance enhancement were averaged from triplicate experiments, and the corresponding errors

144 represent one standard deviation. The pseudo-first-order rate constant (k') for GUA decay was determined using the

145 following equation (Huang et al., 2018):

$$ln\,([GUA]_t/[GUA]_0) = -\,k't \qquad \text{(Eq. 1)}$$

147 where [GUA]$_t$ and [GUA]$_0$ are GUA concentrations at time t and 0, respectively. DMB or VL decay rate constants were

148 calculated by replacing GUA with DMB or VL in Eq. 1. The decay rate constants were normalized to the photon flux

149 measured for each experiment through dividing k' by the measured 2-nitrobenzaldehyde (2NB; a chemical actinometer)

150 decay rate constant, j(2NB) (Mabato et al., 2022). In addition, the decay rate constants were corrected for the internal light

151 screening due to DMB, VL, and AN (Leifer, 1988; Zhang and Anastasio, 2003; Smith et al., 2014, 2016). The values of the

152 internal light screening factor (S_λ) determined around the peak in the light absorption action spectrum (DMB: 310-335 nm,

153 VL: 304-364 nm, nitrate: 300-331 nm) (Smith et al., 2014, 2016) for an 8.5 cm cell were 0.95 for GUA+AN, 0.51 for

154 GUA+DMB, 0.54 for GUA+DMB+AN, 0.57 for GUA+VL, and 0.59 for GUA+VL+AN. Moreover, two independently

155 prepared samples for each reaction condition were analyzed using UHPLC-HESI-Orbitrap-MS. Only peaks that were

156 reproducibly detected in both sets of samples were considered. For clarity, the formulas discussed in this work correspond to

157 neutral analytes (e.g., with H$^+$ or NH$_4^+$ removed from the ion formula). The details of the analytical procedures are provided

158 in the Supplement (Sects. S1 to S4).

159 **2.2 Calculation of the normalized abundance of products**

160 Several recent studies have used comparisons of relative abundance of products based on peak areas from mass spectrometry

161 (MS) results (e.g., Lee et al., 2014; Romonosky et al., 2017; Wang et al., 2017; Fleming et al., 2018; Song et al., 2018; Klodt

162 et al., 2019; Ning et al., 2019) to show the relative importance of different types of compounds (K. Wang et al., 2021).

163 However, comparisons of relative abundance among different compounds can be subject to uncertainties as ionization

164 efficiencies in soft ionization, such as ESI, may significantly vary between different compounds (Kebarle, 2000; Schmidt et

165 al., 2006; Leito et al., 2008; Perry et al., 2008; Kruve et al., 2014). ~~The normalized abundance of products ([P], unitless) was~~

166 ~~introduced in our previous work (Mabato et al., 2022).~~ In our previous work (Mabato et al., 2022), we introduced the

167 normalized abundance of products ([P], unitless) (Eq. 2) as a semi-quantitative analysis that gives an overview of how the

168 signal intensities changed under different experimental conditions but not the quantification of the absolute product

169 concentration. ~~Briefly,~~ The calculation assumes equal ionization efficiencies of different compounds, which is commonly

170 used to estimate O:C ratios of SOA (Bateman et al., 2012; Lin et al., 2012; Laskin et al., 2014; De Haan et al., 2019) ~~was~~

171 ~~assumed for the calculation~~:

172

173 $$[P] = \frac{A_{P,t}}{A_{GUA,t}} \cdot \frac{[GUA]_t}{[GUA]_0} \qquad \text{(Eq. 2)}$$

174 where $A_{P,t}$ and $A_{GUA,t}$ are the extracted ion chromatogram (EIC) peak areas of the product P and GUA from UHPLC-HESI-

175 Orbitrap-MS analyses at time t, respectively; $[GUA]_t$ and $[GUA]_0$ are the GUA concentrations (μM) determined using

176 UHPLC-PDA at time t and 0, respectively. Note that the normalized abundance of products has intrinsic uncertainties due to

177 the variability in ionization efficiencies for various compounds. ~~Nevertheless, it is a semi-quantitative analysis that gives an~~

178 ~~overview of how the signal intensities changed under different experimental conditions but not the quantification of the~~

179 ~~absolute product concentration.~~ Moreover, it should be noted that the normalized abundance of products was calculated

180 using only the positive ion mode data as the GUA signal from the negative ion mode was weak and thus may present large

181 uncertainties during normalization. Therefore, products that may not give signals or may have weak signals in the positive

182 ion mode were possibly underestimated in the normalized product abundance. Nevertheless, it enables the comparison of MS

183 results among different experiments. As demonstrated in our previous work (Mabato et al., 2022) and the current study, a

184 higher normalized abundance of products generally correlates with higher efficiency of oxidation. The reported uncertainties

185 were propagated from the changes in [GUA] measured using UHPLC-PDA and the MS signal intensities.

186

3 Results and Discussion

188 Using kinetics data, MS analyses, and absorbance enhancement data, we first examined the differences between GUA+DMB

189 and GUA+VL (Sect. 3.1). Then, we analyzed GUA+DMB+AN, GUA+VL+AN, and GUA+AN (Sect. 3.2) to explore the

190 effects of nitrate photolysis and ammonium on photosensitized aqSOA formation.

3.1 Comparison of photosensitized GUA oxidation by non-phenolic (^{3}DMB*) and phenolic (^{3}VL*) methoxybenzaldehydes

Prior studies have reported that photosensitized non-carbonyl phenol oxidation in the presence of 3,4-dimethoxybenzaldehyde (DMB) and vanillin (VL) (separately) was mainly driven by ^{3}DMB* and ^{3}VL*, respectively (Smith et al., 2014; Mabato et al., 2022), while contributions from secondary oxidants such as $^1O_2$ and $\cdot$OH were likely minor. However, both ^{3}DMB* and ^{3}VL* are efficiently quenched by O_2, suggesting that energy transfer should be considered in evaluating photosensitized processes involving these methoxybenzaldehydes (Felber et al., 2021). Moreover, it was found that ^{3}DMB*, $^1O_2$, and $O_2^{\cdot-}$ were the major contributors to the photosensitized oxidation of 4-ethylguaiacol (Chen et al., 2020). Recently, the oxidation of guaiacyl acetone (a non-conjugated phenolic carbonyl) in the presence of DMB has been reported to be initiated by ^{3}DMB*, $^1O_2$, $\cdot$OH, or methoxy radical ($\cdot$OCH$_3$) (Misovich et al., 2021). Further studies are thus required to identify the specific oxidants in these reaction systems. In this study, reactions initiated in the presence of DMB or VL are collectively referred to as photosensitized reactions. The reaction conditions, initial guaiacol (GUA) and DMB or VL decay rate constants, normalized product abundance, and the chemical characteristics of aqSOA formed in this work are summarized in Table 1.

3.1.1 Kinetic analysis of photosensitization by ^{3}DMB* and ^{3}VL*

No significant loss of GUA or photosensitizers was observed for dark experiments ($p > 0.05$). Figure S1 shows the decay of GUA, DMB, and VL under different experimental conditions. Upon irradiation, the GUA decay rate constant in GUA+DMB was ~4 times higher than in GUA+VL. In GUA+DMB, the decay rate constant of GUA was ~8 times higher than that of DMB, consistent with a previous study (Smith et al., 2014). Contrastingly, the decay rate constant of VL was 2.4 times higher than that of GUA in GUA+VL. This VL consumption was also observed in our earlier work using 0.1 mM GUA + 0.1 mM VL (Mabato et al., 2022). These trends could be explained by the following reasons. First, DMB has a stronger photosensitizing ability than VL based on its higher quantum yield of ^{3}C* formation and longer lifetime of ^{3}DMB* compared to ^{3}VL* (Felber et al., 2021). Second, VL is also a phenolic compound similar to GUA, and is therefore highly reactive towards oxidation. For instance, its –OH group can be oxidized by ^{3}VL* via H-atom abstraction to form phenoxy radicals which can undergo coupling to form oligomers (Kobayashi and Higashimura, 2003; Sun et al., 2010; Mabato et al., 2022). The faster consumption of VL than GUA suggests a competition between ground-state VL and GUA for reaction with ^{3}VL*. Moreover, compared to a –OCH$_3$ group (in DMB), an –OH group (in VL) has a stronger electron-donating ability and is thus more activating towards. Relative to DMB, VL is more reactive towards electrophilic addition of $\cdot$OH and electrophilic aromatic substitution. It should be noted that the differences in the GUA decay rate constants among different reaction systems are not quantitatively equivalent to photosensitizing efficiencies, and a detailed quantitative analysis of which is beyond the scope of this study. Nonetheless, these results suggested that GUA oxidation in GUA+DMB was overall more efficient than in GUA+VL. Our kinetic analysis focused on the decay rate constants of the aqSOA precursor (GUA) and the photosensitizers (DMB and VL) during photosensitization under the same experimental conditions (same aqSOA

7

224 precursor and concentration, same photosensitizer concentration, and same lamp photon flux). The effects of other factors
225 (e.g., intersystem crossing efficiency) on the rate constants were not examined. Explicit kinetic studies (e.g., Smith et al.,
226 2014, 2015) that measure second-order rate constants should be conducted in the future to extend the applicability of the
227 kinetic parameters to other conditions.

228 **3.1.2 Product distributions and chemical characteristics of aqSOA from photosensitization by ^{3}DMB* and ^{3}VL***

229 The products detected using UHPLC-HESI-Orbitrap-MS were used to characterize~~represent~~ the aqSOA formed in this work.
230 The signal-weighted distributions of aqSOA calculated from combined positive (POS) and negative (NEG) ion modes MS
231 results are summarized in Figure 2. The signal-weighted distributions calculated separately from POS and NEG ion modes
232 MS results are available in Figures S1~~2~~ and S3~~2~~. It should be noted that in this work, the product distributions for all
233 experiments were based on the same irradiation time of 180 min. An irradiation time of 180 min was chosen as it was
234 sufficient to show the differences in the extent of reaction of GUA among the reaction systems studied. For reaction systems
235 with precursors of different reactivities, chemical analysis at a fixed reaction time may be looking at different generations of
236 products of each precursor, as Yu et al. (2014) reported. Measuring the product distribution at a fixed time might have
237 missed the information on what/how many products are formed at the similar amounts of precursors reacted. The situation
238 could be even more complicated if different precursors had major differences in pathways and dominant intermediates.
239 However, comparing the product distributions after a certain time of light exposure, as is the case for this study, is useful to
240 evaluate what products would form after a certain time of photosensitization. Oligomers and derivatives of GUA dominated
241 both GUA+DMB and GUA+VL, in agreement with pronounced oligomerization from triplet-mediated oxidation of
242 relatively high phenol concentration (e.g., 0.1 to 3 mM; Li et al., 2014; Yu et al., 2014, 2016; Slikboer et al., 2015; Ye et al.,
243 2019; Mabato et al., 2022). ~~GUA+DMB had a higher oligomer contribution than GUA+VL, attributable to faster GUA~~
244 ~~oxidation by ^{3}DMB*.~~ Figure 3 schematically depicts the main differences between photosensitized GUA oxidation by
245 ^{3}DMB* and ^{3}VL* in the absence and presence of AN. As shown in Fig. 3, ^{3}DMB* and ^{3}VL* can oxidize GUA via H-atom
246 abstraction to form phenoxy radicals which undergo coupling to form oligomers (Kobayashi and Higashimura, 2003; Sun et
247 al., 2010; Mabato et al., 2022). The higher oligomer contribution in GUA+DMB is likely due to the better photosensitizing
248 ability of DMB than VL and partly the lower abundance of ^{3}VL* due to fast VL consumption. VL was consumed faster than
249 DMB during GUA oxidation ascribable to the –OH group of VL, making it more susceptible to oxidation and more reactive
250 towards electrophilic aromatic substitution. In addition, the normalized product abundance for GUA+DMB was ~4 times
251 higher than that for GUA+VL (Table 1), further suggesting more efficient photosensitized GUA oxidation by ^{3}DMB* than
252 by ^{3}VL*. The oxidation of GUA or transient organic intermediates by secondary oxidants (e.g., ^{1}O$_2$ and $^•$OH) from ^{3}DMB* or
253 ^{3}VL* and the fragmentation of larger compounds generate highly oxidized ring-opening products (Yu et al., 2014; Huang et
254 al., 2018; Chen et al., 2020). GUA+DMB had a higher contribution of ring-opening products than GUA+VL, likely due to
255 the greater availability of secondary oxidants in the former and fast VL consumption lowering the production of these
256 species in GUA+VL. The IC analyses also indicate the formation of small organic acids (e.g., formic acid), which appeared

8

257 to have higher concentrations in the presence of DMB than in VL (Fig. S43). Although no data is available for the
258 concentration changes (every 30 min) of small organic acids during the reaction, it is likely that an increasing trend would be
259 observed as fragmentation, which leads to the decomposition of initially formed oligomers and the generation of smaller
260 oxygenated products, becomes important at longer irradiation times (Huang et al., 2018). This trend has also been observed
261 in our previous work on the direct photosensitized oxidation of VL (Mabato et al., 2022), as well as other studies on
262 photosensitized oxidation of non-carbonyl phenols and phenolic carbonyls (e.g., Yu et al., 2016; Jiang et al., 2021). The
263 reactions of secondary oxidants or ring-opening products with GUA can form functionalized products. Notably, the
264 contribution of monomers in GUA+VL was almost twice as high as in GUA+DMB, ascribable to VL transformation
265 products. We previously showed that for the direct photosensitized oxidation of VL, functionalization prevails over
266 oligomerization at 0.01 mM VL, the [VL] used in this work, while oligomerization dominates at higher [VL] (0.1 mM;
267 Mabato et al., 2022).

268 It has been reported that oligomerization could occur during the electrospray ionization process (Yasmeen et al.,
269 2010). In this work, it was confirmed that the oligomers observed were generated in the solutions via aqueous reactions
270 instead of being artefacts of HESI-MS. This is based on the absence of dimers and higher oligomers in the HESI mass
271 spectra of dark control solutions acquired by direct infusion (Yu et al., 2016).

272 The major GUA+DMB and GUA+VL products (Tables S1-S2) are mostly oligomers which can be formed through
273 the coupling of phenoxy radicals (Kobayashi and Higashimura, 2003; Sun et al., 2010; Mabato et al., 2022). GUA+DMB
274 products matched those reported in previous works on ^{3}DMB*- and/or ·OH-mediated phenol oxidation (Yu et al., 2014,
275 2016). These include GUA dimers and trimers (e.g., $C_{14}H_{14}O_4$ and $C_{21}H_{18}O_8$, #1 and 19; Table S1), aldehydes ($C_7H_6O_4$, #13;
276 Table S1), and esters ($C_{16}H_{18}O_6$, #14; Table S1). Functionalized products include $C_{11}H_{12}O_5$ and $C_{10}H_{12}O_3$ (#8 and 12; Table
277 S1). More than half of the major GUA+VL products are the same oligomers detected from GUA+DMB (e.g., $C_{13}H_{10}O_4$ and
278 $C_{20}H_{18}O_6$, #4 and 21; Table S1). The rest are mainly functionalized species such as $C_7H_8O_4$ and $C_8H_8O_5$ (#28 and 35; Table
279 S2), corresponding to a hydroxylated GUA and hydroxylated VL, respectively.

280 The average elemental ratios and elemental distribution of the products (Fig. S54a–d) were consistent with those in
281 previous studies on similar reaction systems (Yu et al., 2014, 2016; Mabato et al., 2022). The majority of the GUA+DMB
282 and GUA+VL products had H:C ≤1.0 and O:C ≤0.5, typical for aromatic species (Mazzoleni et al., 2012; Kourtchev et al.,
283 2014; Jiang et al., 2021). GUA+DMB had more compounds with higher O:C (≥0.6), in agreement with higher contributions
284 of ring-opening products than in GUA+VL (Fig. 2). The higher ⟨OS_C⟩ for GUA+VL than in GUA+DMB (Table 1) was
285 probably due to the significant functionalization in the former. Moreover, the distributions of OS_C and carbon number (Fig.
286 S65a–d) show that these aqSOA products have similar elemental composition to those of low-volatility oxygenated organic
287 aerosols (LV-OOA), semi-volatile oxygenated organic aerosols (SV-OOA), and slightly with biomass burning organic
288 aerosols (BBOA) (Kroll et al., 2011). Further discussions on van Krevelen diagrams (Fig. S54a–d) and OS_C vs. carbon
289 number plots (Fig. S65a–d) for GUA+DMB and GUA+VL aqSOA are available in the Supplement (Sect. S5). In brief,
290 ^{3}DMB*-initiated GUA oxidation was faster and yielded higher normalized product abundance than oxidation by ^{3}VL*. This

291 is likely due to the stronger photosensitizing ability of DMB than VL and the –OH group of VL facilitating its rapid

292 consumption. In addition, oligomerization and functionalization dominated in both GUA+DMB and GUA+VL, as reported

293 in similar studies (Yu et al., 2014, 2016; Chen et al., 2020; Jiang et al., 2021; Misovich et al., 2021; Mabato et al., 2022).

294 However, functionalization was more prominent in the latter, attributable to the transformation of VL. Nonetheless, it must

295 be noted that for phenolic aqSOA, fragmentation will ultimately be more predominant at longer irradiation times (Huang et

296 al., 2018; Yu et al., 2016; Mabato et al., 2022).

3.1.3 Light absorption of aqSOA from photosensitization by ^{3}DMB* and ^{3}VL*

298 The absorbance enhancement of phenolic aqSOA generated via reactions with ^{3}DMB*/^{3}VL* has been linked to the

299 formation of conjugated structures due to oligomerization and functionalization (e.g., additions of hydroxyl and carbonyl

300 groups; Yu et al., 2014, 2016; Smith et al., 2016; Chen et al., 2020; Jiang et al., 2021; Misovich et al., 2021; Mabato et al.,

301 2022). Moreover, the aqueous-phase photo-oxidation of BB emissions can enhance BrC absorbance via the formation of

302 aromatic dimers and functionalized products (Hems et al., 2020). The increase in light absorption throughout 180 min of

303 irradiation and the change in the rate of sunlight absorption (ΔR_{abs}) (Jiang et al., 2021) from 350 to 550 nm at 180 min during

304 typical clear and haze days in Beijing, China for all the reaction systems studied are provided in Figure 4. Figure S7 shows

305 the absorption spectra after 180 min of irradiation for each reaction system studied. In this work, the absorbance

306 enhancement of GUA+DMB and GUA+VL (Fig. 4a) could be due to~~correlates with~~ oligomers and functionalized

307 monomers, which are the highest contributors to the product signals. ~~–~~Identifying the chromophores responsible for the

308 absorbance enhancement may be beneficial in understanding the impact of aqSOA on the Earth's radiative balance and

309 determining the reactions that affect light absorption by aqSOA (Mabato et al., 2022). However, the detected products did

310 not exhibit distinct peaks in the UHPLC-PDA chromatograms, likely due to the concentration of the chromophores being

311 below the detection limit of PDA. Nevertheless, the higher absorbance enhancement and ΔR_{abs} for GUA+DMB than

312 GUA+VL was ~~most likely associated with~~ probably due to the higher contribution and normalized abundance (by ~6 times)

313 of oligomers in the former.

314 Additional information about aqSOA light-absorption can be deduced from the plots of the double bond equivalent

315 (DBE) values vs. carbon number (n_C) (Lin et al., 2018). Figure S~~6~~8 shows these plots along with the DBE reference values

316 of fullerene-like hydrocarbons (Lobodin et al., 2012), cata-condensed polycyclic aromatic hydrocarbons (PAHs; Siegmann

317 and Sattler, 2000), and linear conjugated polyenes with a general formula C_xH_{x+2}. The shaded area indicates a sufficient level

318 of conjugation for visible light absorption, and species within this region are potential BrC chromophores. GUA+DMB and

319 GUA+VL aqSOA exhibited a significant overlap in the DBE vs. n_C space; nearly all products from both systems, including

320 the high-relative-abundance species, are potential BrC chromophores. GUA+DMB had more oligomeric products with high

321 relative abundance ($n_C \geq 12$ and DBE ≥ 8). For GUA+VL, high-relative-abundance products also include monomeric species

322 ($n_C = 7$-8 and 4-5 DBE) corresponding to hydroxylated products (e.g., $C_7H_8O_4$ and $C_8H_8O_5$; 28 and 35; Table S2). These

323 observations further indicate the importance of oligomerization and functionalization for the absorbance enhancement of

10

324 aqSOA generated via photosensitization by ^{3}DMB* and ^{3}VL*. In summary, ^{3}DMB* and ^{3}VL* can oxidize GUA resulting in

325 aqSOA and BrC formation, but GUA+DMB products exhibited stronger light absorption. In GUA+VL, the extent of GUA

326 oxidation was limited by significant VL consumption.

3.2 Comparison of photosensitized GUA oxidation by non-phenolic (^{3}DMB*) and phenolic (^{3}VL*) methoxybenzaldehydes in the presence of AN

3.2.1 Kinetic analysis of photosensitization by ^{3}DMB* and ^{3}VL* in the presence of AN

330 Ammonium nitrate (AN) did not significantly affect ($p >$ 0.05) the decay rate constants of GUA, DMB, and VL for both

331 GUA+DMB+AN and GUA+VL+AN (Table 1), likely due to the higher molar absorptivities of the photosensitizers

332 compared to that of nitrate. This implies that the chemistry of ^{3}DMB* and ^{3}VL* dominated that of nitrate. In this work, the

333 GUA decay rate constants decreased in the order of GUA+DMB/GUA+DMB+AN > GUA+VL/GUA+VL+AN > GUA+AN

334 (Table 1). Note that as the molar absorptivities of the photosensitizers are higher than that of nitrate, the kinetics data were

335 also analyzed on a per-photon-absorbed basis for a more appropriate comparison of reaction efficiency (Sect. S6). The

336 apparent quantum efficiency of GUA photodegradation (φ_{GUA}) in the presence of nitrate (GUA+AN: 0.17~~1.3 × 10^{-2}~~ ± 3~~2.8~~9 ×

337 10^{-2}~~3~~) was ~2 and ~7 times higher than that in the presence of DMB (0.10~~7.2 × 10^{-3}~~ ± 2~~1~~.9 × 10^{-4}~~3~~) or VL (0.026~~1.8 × 10^{-3}~~ ±

338 74.2~~9~~ × 10^{-4}~~3~~), respectively. This suggests that nitrate-mediated GUA photo-oxidation is more efficient than

339 photosensitization by ^{3}DMB* or ^{3}VL* on a per-photon-absorbed basis.

3.2.2 Product distributions and chemical characteristics of aqSOA from photosensitization by ^{3}DMB* and ^{3}VL* in the presence of AN

342 For both GUA+DMB+AN and GUA+VL+AN, AN had no significant effect on the normalized product abundance (Table 1),

343 but it induced the formation of N-containing products composed of N-heterocycles (e.g., imidazoles and pyridines) and

344 oligomers, as well as nitrated species. Similarly, we previously reported a potential imidazole derivative from the direct

345 photosensitized oxidation of VL in the presence of AN, which was attributed to the reaction of ring-opening products with

346 dissolved ammonia (Mabato et al., 2022). Oligomers remained the highest signal contributors in the presence of AN (Fig. 2),

347 but interactions between photosensitization by ^{3}DMB* and ^{3}VL* and AN photolysis were distinct. First, nitrated species had

348 similar contributions in both cases, but the contribution and normalized abundance of all N-containing products in

349 GUA+DMB+AN were 2 and ~14 times higher, respectively, than in GUA+VL+AN. This difference can be attributed to the

350 higher contribution of N-heterocycles and N-containing oligomers in GUA+DMB+AN. Compared to GUA+VL,

351 GUA+DMB had a higher contribution of ring-opening products which can react with ammonia, as discussed earlier (Figs. 2

352 and 3). Second, the decrease in oligomers in GUA+DMB+AN may be due to their fragmentation induced by •OH from

353 nitrate photolysis, then conversion to N-containing products. Correspondingly, the contribution of possibly ring-retaining N-

354 containing products in GUA+DMB+AN (18.6%) was ~3 times higher than that in GUA+VL+AN (6.5%). While

355 fragmentation of oligomers likely occurred in GUA+VL+AN as well, the increase in oligomers suggests that other reactions

11

356 have taken place. For GUA+VL+AN, $^\bullet$OH or $^\bullet$NO$_2$ from nitrate photolysis may have initiated H-atom abstraction from the –

357 OH group of VL, generating phenoxy radicals which can undergo coupling to form more oligomers (Kobayashi and

358 Higashimura, 2003; Sun et al., 2010; Mabato et al., 2022). This may also explain the more significant decrease of monomers

359 in GUA+VL+AN (~3 times) compared to GUA+DMB+AN (~2 times). Similarly, we previously observed an increase in

360 oligomers during the direct photosensitized oxidation of upon adding 1 mM AN to 0.01 mM VL (Mabato et al., 2022), the

361 [VL] used in this work, upon adding 1 mM AN. These findings indicate that photosensitization by non-phenolic and

362 phenolic methoxybenzaldehydes may interact differently with AN photolysis.

363   GUA+AN mainly formed oligomers analogous to $^\bullet$OH-mediated phenol oxidation (Yu et al., 2014, 2016), followed

364 by N-containing products. The normalized product abundance of GUA+AN was the lowest among all experiments, likely

365 due to the lower GUA decay constant relative to photosensitized oxidation. Moreover, the normalized abundance of N-

366 containing products in GUA+AN was ~12 times lower than that in GUA+DMB+AN but comparable to that in

367 GUA+VL+AN. This discrepancy for GUA+VL+AN might be due to the weaker signals of its N-containing products in the

368 positive compared to the negative ion mode. As previously mentioned, the normalized product abundance was calculated

369 using only the positive ion mode data as the GUA signal from the negative ion mode was weak and thus may present large

370 uncertainties during normalization. Interestingly, the contributions from nitrated species in GUA+DMB+AN and

371 GUA+VL+AN were higher than in GUA+AN, suggesting possible enhancement of nitration reactions. This is likely due to

372 the increased formation of $^\bullet$NO$_2$, for instance, via the reactions of $^\bullet$OH and O$_2$$^{\bullet-}$ (from ^{3}DMB* or ^{3}VL*) with NO$_2^-$ (Pang et

373 al., 2019; Mabato et al., 2022). Similarly, we previously reported enhanced nitration via the direct photosensitized oxidation

374 of VL in the presence of AN under air-saturated conditions (O$_2$ is present) relative to nitrogen-saturated conditions (Mabato

375 et al., 2022). Theseis implyies that photosensitizationed reactions may promote reactions induced by nitrate photolysis.

376   The major products from GUA+DMB+AN, GUA+VL+AN, and GUA+AN (Tables S3–S5) include oligomers and

377 functionalized monomers detected in GUA+DMB and GUA+VL (Tables S1–S2). The N-heterocycles from

378 GUA+DMB+AN include C$_6$H$_6$N$_4$ (#41; Table S3), which may be 2,2'-biimidazole (BI), a reaction product from glyoxal +

379 reduced nitrogenous compounds (e.g., ammonium salts) (De Haan et al., 2009; Galloway et al., 2009; Nozière et al., 2009;

380 Shapiro et al., 2009; Yu et al., 2011; Kampf et al., 2012; Gen et al., 2018; Mabato et al., 2019). The nitrated products include

381 C$_{12}$H$_{11}$N$_3$O$_3$ and C$_{15}$H$_{10}$N$_4$O$_3$ (#42 and 49; Table S3), which possibly have a nitrated imidazole moiety and a nitrophenol

382 moiety, respectively. For GUA+VL+AN, oligomers (C$_{14}$H$_{12}$O$_6$ and C$_{20}$H$_{16}$O$_7$; #55 and 59, Table S4) which were not among

383 the major products in GUA+VL were noted. C$_{10}$H$_8$O$_2$ likely has a furanone group (#50; Table S4); furanones are the primary

384 products of the reaction of $^\bullet$OH with toluene and other aromatic hydrocarbons (Smith et al., 1999). Moreover, C$_{11}$H$_9$N$_3$O$_3$

385 (#57; Table S4) has a nitrated imidazole moiety. Among the N-containing compounds in GUA+AN is C$_4$H$_3$N$_3$O$_3$ (#69; Table

386 S5), which may be a nitrated imidazole-2-carboxaldehyde. Imidazole-2-carboxaldehyde is also a reaction product from

387 glyoxal + reduced nitrogenous compounds (e.g., ammonium salts) (De Haan et al., 2009; Galloway et al., 2009; Nozière et

388 al., 2009; Shapiro et al., 2009; Yu et al., 2011; Kampf et al., 2012; Gen et al., 2018; Mabato et al., 2019).

389   The ⟨O:C⟩ for GUA+DMB+AN and GUA+VL+AN were lower than those in the absence of AN (Table 1), ~~likely~~
390 ~~due to the rapid formation of highly oxidized species followed by their decomposition (Huang et al., 2018)~~ possibly due to
391 the formation of N-heterocycles, altering the elemental ratios. The ⟨O:C⟩ and ⟨H:C⟩ were comparable in GUA+DMB+AN
392 and GUA+VL+AN, but the ⟨N:C⟩ for the former was higher, implying a greater extent of reactions involving AN. Relative
393 to GUA+DMB+AN and GUA+VL+AN, GUA+AN had a higher ⟨N:C⟩, as can be expected given that AN was the only
394 oxidant source. The lower ⟨OS$_C$⟩ of GUA+DMB+AN and GUA+VL+AN compared to GUA+AN may be attributed to
395 triplet-initiated oxidation generating higher-molecular-weight products with less fragmentation compared to ·OH-mediated
396 oxidation (Yu et al., 2014; Chen et al., 2020). Nonetheless, AN generally increased the ⟨OS$_C$⟩ for both GUA+DMB and
397 GUA+VL, with a more noticeable increase for the former, suggesting more oxidized products. Similarly, in a previous work,
398 the more oxygenated and oxidized aqSOA from the photo-oxidation of phenolic carbonyls in AN solutions than in
399 ammonium sulfate solutions has been ascribed to nitrate photolytic products promoting the reactions (Huang et al., 2018).
400 Furthermore, GUA+DMB+AN and GUA+VL+AN aqSOA had mainly similar features in the OS$_C$ vs. n$_C$ plots as those
401 observed in the absence of AN (Fig. S6~~5~~). More information on van Krevelen diagrams (Figs. S5~~4~~e–h and S9~~7~~) and OS$_C$ vs.
402 n$_C$ plots (Figs. S6~~5~~e–h and S10~~8~~) for GUA+DMB+AN, GUA+VL+AN, and GUA+AN aqSOA are provided in the
403 Supplement (Sect. S7). In essence, AN had no significant effect on the decay kinetics ascribable to photosensitizer chemistry
404 prevailing over nitrate, but it induced the formation of N-containing products. Moreover, AN modified the product
405 distributions, albeit in different ways (Figs. 2 and 3). In particular, N-containing products were more abundant in
406 GUA+DMB+AN, probably due to more extensive fragmentation in GUA+DMB than in GUA+VL. In GUA+VL+AN, AN
407 promoted oligomer formation likely via the -OH group of VL. Furthermore, GUA+DMB+AN and GUA+VL+AN had more
408 nitrated products than GUA+AN, suggesting that photosensitized reactions may promote nitrate photolysis-initiated
409 reactions.

410 **3.2.3 Light absorption of aqSOA from photosensitization by [3]DMB* and [3]VL* in the presence of AN**

411 The presence of AN also did not appreciably affect the absorbance enhancement and ΔR$_{abs}$ for both GUA+DMB+AN and
412 GUA+VL+AN (Fig. 4). For GUA+DMB+AN, the N-containing products may have offset the decrease in oligomers to
413 maintain the absorbance enhancement observed from GUA+DMB. Wang et al. (2022) reported that nitration might
414 contribute significantly to absorbance enhancement for methoxyphenols in sodium nitrate ~~(Wang et al., 2022)~~. In
415 GUA+VL+AN, the decrease in monomers may have counteracted the increased oligomers and the generated N-containing
416 products. Compared to GUA+DMB+AN, the N-containing products from GUA+VL+AN probably had less impact on the
417 absorbance enhancement based on their smaller signal contribution.
418   Similar to experiments without AN, CHO species from GUA+DMB+AN and GUA+VL+AN were mainly
419 overlapped in the DBE vs. n$_C$ space (Fig. S8~~6~~c,d) and were mostly potential BrC chromophores. In both systems, GUA
420 dimers were the products with the highest relative abundance. For GUA+DMB+AN, products with high relative abundance
421 also include a CHN species, while two CHON species had high n$_C$ (18,20) and DBE (16,14) values. In GUA+VL+AN,

422 products with high relative abundance include a CHON species (n_C = 11 and 9 DBE). Approximately 30% and 43% of the

423 N-containing products for GUA+DMB+AN and GUA+VL+AN, respectively, were among the potential BrC chromophores.

424 This suggests the possible significance of N-containing products for light absorption of aqSOA from photosensitization by

425 methoxybenzaldehydes and AN photolysis. Correspondingly, nitroaromatic compounds and N-heterocycles are frequently

426 noted in BBOA (Iinuma et al., 2010; Kitanovski et al., 2012; Kourtchev et al., 2016) and have been proposed to be potential

427 contributors to BrC light absorption (Laskin et al., 2015). Relative to GUA+DMB+AN and GUA+VL+AN, only 19% of the

428 N-containing products in GUA+AN were potential BrC chromophores (Fig. S86e,f), and these did not include CHN species.

429 These indicate that the N-containing products formed in the presence of both photosensitizers and AN may be more

430 significant contributors to the light absorption of phenolic aqSOA than those formed in AN only.

431 **4 Conclusions and atmospheric implications**

432 The photosensitized oxidation of guaiacol (GUA) by triplet excited states of 3,4-dimethoxybenzaldehyde ([3]DMB*) and

433 vanillin ([3]VL*) (separately) in the absence and presence of ammonium nitrate (AN) were compared under identical

434 conditions (simulated sunlight and concentration) relevant to atmospheric cloud and fog waters. Compared to GUA+VL,

435 faster GUA oxidation and stronger light absorption by the products were observed in GUA+DMB. Moreover, VL was

436 consumed faster relative to DMB, limiting the extent of GUA oxidation in GUA+VL. These differences are rooted in DMB

437 having a better photosensitizing ability than VL and the –OH group of VL, making it more susceptible to oxidation and more

438 reactive towards electrophilic aromatic substitution. Both GUA+DMB and GUA+VL generated aqSOA (, including potential

439 BrC chromophores) composed of oligomers, functionalized monomers, oxygenated ring-opening products, and N-containing

440 products in the presence of AN. The major aqSOA formation processes for GUA+DMB and GUA+VL were oligomerization

441 and functionalization, but functionalization appeared to be more significant in GUA+VL due to VL transformation products.

442 The photochemical evolution of aqSOA from GUA+DMB has been reported by Yu et al. (2016). Similar experiments for

443 aqSOA from GUA+VL should be conducted in the future to better understand photosensitized reactions involving phenolic

444 carbonyl photosensitizers.

445 AN did not significantly affect the decay kinetics due to the predominant effect of [3]DMB* and [3]VL* chemistry

446 compared to nitrate, but it promoted the formation of N-containing products; these are composed of N-heterocycles (e.g.,

447 imidazoles) and oligomers and nitrated species. The observation of N-heterocycles agrees with our previous findings that

448 ammonium participates in photosensitized oxidation of phenolic compounds in the presence of AN (Mabato et al., 2022).

449 These results also suggest that photosensitized oxidation of phenolic compounds in the presence of AN might be an

450 important source of N-heterocycles and nitrated products. Identifying the sources of N-heterocycles and nitrated compounds

451 is important due to their environmental and health impacts (Laskin et al., 2009). Moreover, photosensitized reactions by non-

452 phenolic and phenolic methoxybenzaldehydes may be differently influenced by AN photolysis. For instance, the more

453 extensive fragmentation in GUA+DMB than in GUA+VL possibly resulted in more N-containing products in

14

454   GUA+DMB+AN. Furthermore, the increased oligomers in GUA+VL+AN may be due to VL-derived phenoxy radicals

455   induced by $^{\bullet}$OH or $^{\bullet}$NO$_2$ from nitrate photolysis. In addition, more nitrated compounds observed in GUA+DMB+AN and

456   GUA+VL+AN than in GUA+AN imply that photosensitized reactions may promote nitrate-mediated photolytic reactions.

457   On a related note, the significance of photosensitization by BrC (via formation of solvated electrons; Y. Wang et al., 2021)

458   and marine dissolved organic matter (via O$_2^{\bullet-}$ formation; Garcia et al., 2021) in enhanced nitrite production from nitrate

459   photolysis have been reported. A recent study from our group has shown that glyoxal photo-oxidation mediated by both

460   nitrate photolysis and photosensitization can significantly enhance the atmospheric sink of glyoxal (Zhang et al., 2022).

461   Further studies are needed to improve our understanding of the interplay between photosensitized reactions and nitrate

462   photolysis.

463   This study demonstrates that the structural features of photosensitizers affect aqSOA formation via non-carbonyl

464   phenol oxidation. The VL results are broadly relevant to other phenolic carbonyls, but the effects of different functional

465   groups should still be considered. For instance, the aldehyde/ketone pair of syringaldehyde and acetosyringone, both

466   phenolic carbonyls, have been reported to have equal reactivity towards direct photosensitized oxidation. This is due to the

467   greater light absorption by the aldehyde form but higher quantum efficiency for loss for the ketone form (Smith et al. 2016).

468   However, more aqSOA was observed from syringaldehyde than acetosyringone (in either AN or ammonium sulfate; Huang

469   et al., 2018). Our findings also imply that while the contributions of photosensitization by ^{3}VL* (and other phenolic

470   carbonyls) to aqSOA formation would be relatively less compared to that of ^{3}DMB* (and other non-phenolic carbonyls),

471   these are not negligible. As both non-phenolic and phenolic carbonyls such as the methoxybenzaldehydes examined in this

472   work are emitted in large amounts from biomass burning, future experiments should probe the aqSOA contribution of a

473   wider variety of photosensitizers. Moreover, further experiments on photosensitized reactions in authentic particulate matter

474   (PM) samples should be conducted in the future. Multicomponent reactions such as GUA+DMB+AN and GUA+VL+AN

475   should also be explored for a more accurate simulation of ambient conditions. These would be useful in assessing the overall

476   impact of photosensitized reactions and AN photolysis on aqSOA formation in areas impacted by biomass burning and high

477   AN concentrations, and for their better representation in aqSOA models.

478

479   *Data availability.*

480   The data used in this publication are available to the community and can be accessed by request to the corresponding author.

481   *Author contributions.*

482   BRGM designed and conducted the experiments; BRGM and CKC wrote the paper. All co-authors contributed to the

483   discussion of the manuscript.

484   *Competing interests.*

485   The authors declare that they have no conflict of interest.

486   *Acknowledgments.*

References

494 Anastasio, C., Faust, B. C., and Rao, C. J.: Aromatic carbonyl compounds as aqueous-phase photochemical sources of
495 hydrogen peroxide in acidic sulfate aerosols, fogs, and clouds. 1. Non-phenolic methoxybenzaldehydes and
496 methoxyacetophenones with reductants (phenols), Environ. Sci. Technol., 31, 218−232, https://doi.org/10.1021/es960359g,
497 1997.

499 Bateman, A. P., Laskin, J., Laskin, A., and Nizkorodov, S. A.: Applications of high-resolution electrospray ionization mass
500 spectrometry to measurements of average oxygen to carbon ratios in secondary organic aerosols, Environ. Sci. Technol., 46,
501 8315–832, https://doi.org/10.1021/es3017254, 2012.

503 Bianco, A., Passananti, M., Brigante, M., and Mailhot, G.: Photochemistry of the cloud aqueous phase: a review, Molecules,
504 25, 423, https://doi.org/10.3390/molecules25020423, 2020.

506 Calvert, J. G. and Madronich, S.: Theoretical study of the initial products of the atmospheric oxidation of hydrocarbons, J.
507 Geophys. Res., 92, 2211−2220, https://doi.org/10.1029/JD092iD02p02211, 1987.

509 Chen, Y., Li, N., Li, X., Tao, Y., Luo, S., Zhao, Z., Ma, S., Huang, H., Chen, Y., Ye, Z., and Ge, X.: Secondary organic
510 aerosol formation from ^{3}C*-initiated oxidation of 4-ethylguaiacol in atmospheric aqueous-phase, Sci. Total Environ., 723,
511 137953, https://doi.org/10.1016/j.scitotenv.2020.137953, 2020.

513 Chen, Z. and Anastasio, C.: Concentrations of a triplet excited state are enhanced in illuminated ice, Environ. Sci.: Processes
514 Impacts, 19, 12−21, https://doi.org/10.1039/C6EM00534A, 2017.

516 Collett, J. L. Jr., Hoag, K. J., Sherman, D. E., Bator, A., and Richards, L. W.: Spatial and temporal variations in San Joaquin
517 Valley fog chemistry, Atmos. Environ., 33, 129−140, https://doi.org/10.1016/S1352-2310(98)00136-8, 1998.

519 De Haan, D. O., Tolbert, M. A., and Jimenez, J. L.: Atmospheric condensed-phase reactions of glyoxal with methylamine,
520 Geophys. Res. Lett., 36, No. L11819, https://doi.org/10.1029/2009GL037441, 2009.

523 De Haan, D. O., Hawkins, L. N., Kononenko, J. A., Turley, J. J., Corrigan, A. L., Tolbert, M. A., and Jimenez, J. L.:
524 Formation of nitrogen-containing oligomers by methylglyoxal and amines in simulated evaporating cloud droplets, Environ.
525 Sci. Technol., 45, 984−991, https://doi.org/10.1021/es102933x, 2011.

527 De Haan, D. O., Pajunoja, A., Hawkins, L. N., Welsh, H. G., Jimenez, N. G., De Loera, A., Zauscher, M., Andretta, A. D.,
528 Joyce, B. W., De Haan, A. C., Riva, M., Cui, T., Surratt, J. D., Cazaunau, M., Formenti, P., Gratien, A., Pangui, E., and
529 Doussin, J-F.: Methylamine's effects on methylglyoxal-containing aerosol: chemical, physical, and optical changes, ACS
530 Earth Space Chem., 3, 1706–1716, https://doi.org/10.1021/acsearthspacechem.9b00103, 2019.

531

532 ~~De Haan, D. O., Tolbert, M. A., and Jimenez, J. L.: Atmospheric condensed phase reactions of glyoxal with methylamine,~~
533 ~~Geophys. Res. Lett., 36, No. L11819, https://doi.org/10.1029/2009GL037441, 2009.~~

534

535 Du, Y., Fu, Q. S., Li, Y., and Su, Y.: Photodecomposition of 4-chlorophenol by reactive oxygen species in UV/air system, J.
536 Hazard. Mater., 186, 491–496, https://doi.org/10.1016/j.jhazmat.2010.11.023, 2011.

537

538 Edye, L. A. and Richards, G. N.: Analysis of condensates from wood smoke. components derived from polysaccharides and
539 lignins, Environ. Sci. Technol., 25, 1133−1137, https://doi.org/10.1021/es00018a018, 1991.

540

541 Felber, T., Schaefer, T., He, L., and Herrmann, H.: Aromatic carbonyl and nitro compounds as photosensitizers and their
542 photophysical properties in the tropospheric aqueous phase, J. Phys. Chem. A, 125, 5078−5095,
543 https://doi.org/10.1021/acs.jpca.1c03503, 2021.

544

545 Fleming, L. T., Lin, P., Laskin, A., Laskin, J., Weltman, R., Edwards, R. D., Arora, N. K., Yadav, A., Meinardi, S., Blake, D.
546 R., Pillarisetti, A., Smith, K. R., and Nizkorodov, S. A.: Molecular composition of particulate matter emissions from dung
547 and brushwood burning household cookstoves in Haryana, India, Atmos. Chem. Phys., 18, 2461–2480,
548 https://doi.org/10.5194/acp-18-2461-2018, 2018.

549

550 Galloway, M. M., Chhabra, P. S., Chan, A. W. H., Surratt, J. D., Flagan, R. C., Seinfeld, J. H., and Keutsch, F. N.: Glyoxal
551 uptake on ammonium sulphate seed aerosol: reaction products and reversibility of uptake under dark and irradiated
552 conditions, Atmos. Chem. Phys., 9, 3331–3345, https://doi.org/10.5194/acp-9-3331-2009, 2009.

553

554 Garcia, S. L. M., Pandit, S., Navea, J. G., and Grassian, V. H.: Nitrous acid (HONO) formation from the irradiation of
555 aqueous nitrate solutions in the presence of marine chromophoric dissolved organic matter: comparison to other organic
556 photosensitizers, ACS Earth Space Chem., 5, 3056−3064, https://doi.org/10.1021/acsearthspacechem.1c00292, 2021.

557

558 Gen, M., Huang, D. D., and Chan, C. K.: Reactive uptake of glyoxal by ammonium-containing salt particles as a function of
559 relative humidity, Environ. Sci. Technol., 52, 6903−6911, https://doi.org/10.1021/acs.est.8b00606, 2018.

560

561 Gen, M., Zhang, R., Huang, D. D., Li, Y. J., and Chan, C. K.: Heterogeneous SO_2 oxidation in sulfate formation by
562 photolysis of particulate nitrate, Environ. Sci. Technol. Lett., 6, 86–91, https://doi.org/10.1021/acs.estlett.8b00681, 2019a.

563

564 Gen, M., Zhang, R., Huang, D. D., Li, Y. J., and Chan, C. K.: Heterogeneous oxidation of SO_2 in sulfate production during
565 nitrate photolysis at 300 nm: effect of pH, relative humidity, irradiation intensity, and the presence of organic compounds,
566 Environ. Sci. Technol., 53, 8757–8766, https://doi.org/10.1021/acs.est.9b01623, 2019b.

567

568 Gen, M., Liang, Z., Zhang, R., Mabato, B. R. G., and Chan, C. K.: Particulate nitrate photolysis in the atmosphere, Environ.
569 Sci.: Atmos., 2, 111–127, https://doi.org/10.1039/d1ea00087j, 2022.

570

571 George, C., Brüggemann, M., Hayeck, N., Tinel, L., and Donaldson, J.: Interfacial photochemistry: physical chemistry of
572 gas-liquid interfaces, in: Developments in Physical & Theoretical Chemistry, edited by: Faust, J. A. and House, J. E.,
573 Elsevier, 435–457, https://doi.org/10.1016/B978-0-12-813641-6.00014-5, 2018.

574

575 Giulianelli, L., Gilardoni, S., Tarozzi, L., Rinaldi, M., Decesari, S., Carbone, C., Facchini, M. C., and Fuzzi, S.: Fog
576 occurrence and chemical composition in the Po valley over the last twenty years, Atmos. Environ., 98, 394–401,
577 https://doi.org/10.1016/j.atmosenv.2014.08.080, 2014.

578

Grace, D. N., Sharp, J. R., Holappa, R. E., Lugos, E. N., Sebold, M. B., Griffith, D. R., Hendrickson, H. P., and, Galloway, M. M.: Heterocyclic product formation in aqueous brown carbon systems, ACS Earth Space Chem., 3, 2472−2481, https://doi.org/10.1021/acsearthspacechem.9b00235, 2019.

Hawthorne, S. B., Miller, D. J., Langenfeld, J. J., and Krieger, M. S.: PM-10 High-volume collection and quantitation of semi- and nonvolatile phenols, methoxylated phenols, alkanes, and polycyclic aromatic hydrocarbons from winter urban air and their relationship to wood smoke emissions, Environ. Sci. Technol., 26, 2251−2262, https://doi.org/10.1021/es00035a026, 1992.

Hems, R. F., Schnitzler, E. G., Bastawrous, M., Soong, R., Simpson, A. J., and Abbatt, J. P. D.: Aqueous photoreactions of wood smoke brown carbon, ACS Earth Space Chem., 4, 1149−1160, https://doi.org/10.1021/acsearthspacechem.0c0011, 2020.

Hoshino, M., Akimoto, H., and Okuda, M.: Photochemical oxidation of benzene, toluene, and ethylbenzene initiated by OH radicals in the gas phase, Bull. Chem. Soc. Jpn., 51, 718−724, https://doi.org/10.1246/bcsj.51.718, 1978.

Huang, D. D., Zhang, Q., Cheung, H. H. Y., Yu, L., Zhou, S., Anastasio, C., Smith, J. D., and Chan, C. K.: Formation and evolution of aqSOA from aqueous-phase reactions of phenolic carbonyls: comparison between ammonium sulfate and ammonium nitrate solutions, Environ. Sci. Technol., 52, 9215–9224, https://doi.org/10.1021/acs.est.8b03441, 2018.

Iinuma, Y., Böge, O., Gräfe, R., and Herrmann, H.: Methyl-nitrocatechols: atmospheric tracer compounds for biomass burning secondary organic aerosols, Environ. Sci. Technol., 44, 8453–8459, https://doi.org/10.1021/es102938a, 2010.

Jiang, W., Misovich, M. V., Hettiyadura, A. P. S., Laskin, A., McFall, A. S., Anastasio, C., and Zhang, Q.: Photosensitized reactions of a phenolic carbonyl from wood combustion in the aqueous phase—chemical evolution and light absorption properties of aqSOA, Environ. Sci. Technol., 55, 5199−5211, https://doi.org/10.1021/acs.est.0c07581, 2021.

Kampf, C. J., Jakob, R., and Hoffmann, T.: Identification and characterization of aging products in the glyoxal/ammonium sulfate system – implications for light-absorbing material in atmospheric aerosols, Atmos. Chem. Phys., 12, 6323–6333, https://doi.org/10.5194/acp-12-6323-2012, 2012.

Kebarle, P. A.: A brief overview of the mechanisms involved in electrospray mass spectrometry, J. Mass Spectrom., 35, 804−817, https://doi.org/10.1002/9783527628728.ch1, 2000.

Kitanovski, Z., Grgić, I., Vermeylen, R., Claeys, M., and Maenhaut, W.: Liquid chromatography tandem mass spectrometry method for characterization of monoaromatic nitro-compounds in atmospheric particulate matter, J. Chromatogr. A, 1268, 35–43, https://doi.org/10.1016/j.chroma.2012.10.021, 2012.

Klodt, A.L., Romonosky, D.E., Lin, P., Laskin, J., Laskin, A., and Nizkorodov, S.A.: Aqueous photochemistry of secondary organic aerosol of α-pinene and α-humulene in the presence of hydrogen peroxide or inorganic salts, ACS Earth Space Chem., 3, 12, 2736–2746, https://doi.org/10.1021/acsearthspacechem.9b00222, 2019.

Kobayashi, S. and Higashimura, H.: Oxidative polymerization of phenols revisited, Prog. Polym. Sci., 28, 1015–1048, https://doi.org/10.1016/S0079-6700(03)00014-5, 2003.

Kourtchev, I., Fuller, S. J., Giorio, C., Healy, R. M., Wilson, E., O'Connor, I., Wenger, J. C., McLeod, M., Aalto, J., Ruuskanen, T. M., Maenhaut, W., Jones, R., Venables, D. S., Sodeau, J. R., Kulmala, M., and Kalberer, M.: Molecular composition of biogenic secondary organic aerosols using ultrahigh-resolution mass spectrometry: comparing laboratory and field studies, Atmos. Chem. Phys., 14, 2155−2167, https://doi.org/10.5194/acp-14-2155-2014, 2014.

629

630 Kourtchev, I., Godoi, R. H. M., Connors, S., Levine, J. G., Archibald, A. T., Godoi, A. F. L., Paralovo, S. L., Barbosa, C. G.
631 G., Souza, R. A. F., Manzi, A. O., Seco, R., Sjostedt, S., Park, J., Guenther, A., Kim, S., Smith, J., Martin, S. T., and
632 Kalberer, M.: Molecular composition of organic aerosols in central Amazonia: an ultra-high-resolution mass spectrometry
633 study, Atmos. Chem. Phys., 16, 11899–11913, https://doi.org/10.5194/acp-16-11899-2016, 2016.

634

635 Kroll, J. H., Donahue, N. M., Jimenez, J. L., Kessler, S. H., Canagaratna, M. R., Wilson, K. R., Altieri, K. E., Mazzoleni, L.
636 R., Wozniak, A. S., Bluhm, H., Mysak, E. R., Smith, J. D., Kolb, C. E., and Worsnop, D. R.: Carbon oxidation state as a
637 metric for describing the chemistry of atmospheric organic aerosol, Nat. Chem., 3, 133–139,
638 https://doi.org/10.1038/nchem.948, 2011.

639

640 Kruve, A., Kaupmees, K., Liigand, J., and Leito, I.: Negative electrospray ionization via deprotonation: predicting the
641 ionization efficiency, Anal. Chem., 86, 4822–4830, https://doi.org/10.1021/ac404066v, 2014.

642

643 Laskin, A., Smith, J. S., and Laskin, J.: Molecular characterization of nitrogen-containing organic compounds in biomass
644 burning aerosols using high-resolution mass spectrometry, Environ. Sci. Technol., 43, 3764–3771,
645 https://doi.org/10.1021/es803456n, 2009.

646

647 Laskin, A., Laskin, J., and Nizkorodov, S. A.: Chemistry of atmospheric brown carbon, Chem. Rev., 115, 4335–4382,
648 https://doi.org/10.1021/cr5006167, 2015.

649

650 Laskin, J., Laskin, A., Nizkorodov, S. A., Roach, P., Eckert, P., Gilles, M. K., Wang, B., Lee, H. J., and Hu, Q.: Molecular
651 selectivity of brown carbon chromophores, Environ. Sci. Technol., 48, 12047–12055, https://doi.org/10.1021/es503432r,
652 2014.

653

654 Lee, A. K. Y., Zhao, R., Li, R., Liggio, J., Li, S., and Abbatt, J. P. D.: Formation of light absorbing organo-nitrogen species
655 from evaporation of droplets containing glyoxal and ammonium sulfate, Environ. Sci. Technol., 47, 12819−12826,
656 https://doi.org/10.1021/es402687w, 2013.
657 Lee, H. J., Aiona, P. K., Laskin, A., Laskin, J., and Nizkorodov, S. A.: Effect of solar radiation on the optical properties and
658 molecular composition of laboratory proxies of atmospheric brown carbon, Environ. Sci. Technol., 48, 10217–10226,
659 https://doi.org/10.1021/es502515r, 2014.

660

661 Leifer, A.: The Kinetics of environmental aquatic photochemistry: Theory and practice, American Chemical Society,
662 Washington, DC, 1988.

663

664 Leito, I., Herodes, K., Huopolainen, M., Virro, K., Künnapas, A., Kruve, A., and Tanner, R.: Towards the electrospray
665 ionization mass spectrometry ionization efficiency scale of organic compounds, Rapid Commun. Mass Sp., 22, 379–384,
666 https://doi.org/10.1002/rcm.3371, 2008.

667

668 Li, P., Li, X., Yang, C., Wang, X., Chen, J., and Collett, J. L. Jr.: Fog water chemistry in Shanghai, Atmos. Environ., 45,
669 4034−4041, https://doi.org/10.1016/j.atmosenv.2011.04.036, 2011.

670

671 Li, Y. J., Huang, D. D., Cheung, H. Y., Lee, A. K. Y., and Chan, C. K.: Aqueous-phase photochemical oxidation and direct
672 photolysis of vanillin - a model compound of methoxy phenols from biomass burning, Atmos. Chem. Phys., 14, 2871−2885,
673 https://doi.org/10.5194/acp-14-2871-2014, 2014.

674

675 Liang, Z., Zhang, R., Gen, M., Chu, Y., and Chan, C. K.: Nitrate photolysis in mixed sucrose–nitrate–sulfate particles at
676 different relative humidities, J. Phys. Chem. A, 125, 3739–3747, https://doi.org/10.1021/acs.jpca.1c00669, 2021.

677

Lin, P., Yu, J. Z., Engling, G., and Kalberer, M.: Organosulfates in humic-like substance fraction isolated from aerosols at seven locations in East Asia: a study by ultra-high-resolution mass spectrometry, Environ. Sci. Technol., 46, 13118–13127, https://doi.org/10.1021/es303570v, 2012.

Lin, P., Fleming, L. T., Nizkorodov, S. A., Laskin, J., and Laskin, A.: Comprehensive molecular characterization of atmospheric brown carbon by high resolution mass spectrometry with electrospray and atmospheric pressure photoionization, Anal. Chem., 90, 12493–12502, https://doi.org/10.1021/acs.analchem.8b02177, 2018.

Lipari, F., Dasch, J. M., and Scruggs, W. F.: Aldehyde emissions from wood-burning fireplaces, Environ. Sci. Technol., 18, 326−330, https://doi.org/10.1021/es00123a007, 1984.

Liu, C., Chen, D., and Chen, X.: Atmospheric reactivity of methoxyphenols: a review, Environ. Sci. Technol., 56, 2897–2916, https://doi.org/10.1021/acs.est.1c06535, 2022.

Lobodin, V. V., Marshall, A. G., and Hsu, C. S.: Compositional space boundaries for organic compounds, Anal. Chem., 84, 3410–3416, https://doi.org/10.1021/ac300244f, 2012.

Mabato, B. R. G., Gen, M., Chu, Y., and Chan, C. K.: Reactive uptake of glyoxal by methylaminium-containing salts as a function of relative humidity, ACS Earth Space Chem., 3, 150–157, https://doi.org/10.1021/acsearthspacechem.8b00154, 2019.

Mabato, B. R. G., Lyu, Y., Ji, Y., Li, Y. J., Huang, D. D., Li, X., Nah, T., Lam, C. H., and Chan, C. K.: Aqueous secondary organic aerosol formation from the direct photosensitized oxidation of vanillin in the absence and presence of ammonium nitrate, Atmos. Chem. Phys., 22, 273−293, https://doi.org/10.5194/acp-22-273-2022, 2022.

Mazzoleni, L. R., Saranjampour, P., Dalbec, M. M., Samburova, V., Hallar, A. G., Zielinska, B., Lowenthal, D. H., and Kohl, S.: Identification of water-soluble organic carbon in non-urban aerosols using ultrahigh-resolution FT-ICR mass spectrometry: organic anions, Environ. Chem., 9, 285−297, https://doi.org/10.1071/EN11167, 2012.

Minero, C., Bono, F., Rubertelli, F., Pavino, D., Maurino, V., Pelizzetti, E., and Vione, D.: On the effect of pH in aromatic photonitration upon nitrate photolysis, Chemosphere, 66, 650−656, https://doi.org/10.1016/j.chemosphere.2006.07.082, 2007.

Misovich, M. V., Hettiyadura, A. P. S., Jiang, W., Zhang, Q., and Laskin, A.: Molecular-level study of the photo-oxidation of aqueous-phase guaiacyl acetone in the presence of $^3C^*$: formation of brown carbon products, ACS Earth Space Chem., 5, 1983−1996, https://doi.org/10.1021/acsearthspacechem.1c00103, 2021.

Munger, J. W., Jacob, D. J., Waldman, J. M., and Hoffmann, M. R.: Fogwater chemistry in an urban atmosphere, J. Geophys. Res. [Oceans], 88, 5109–5121, https://doi.org/10.1029/JC088iC09p05109, 1983.

Ning, C., Gao, Y., Zhang, H., Yu, H., Wang, L., Geng, N., Cao, R., and Chen, J.: Molecular characterization of dissolved organic matters in winter atmospheric fine particulate matters (PM2.5) from a coastal city of northeast China, Sci. Total Environ., 689, 312–321, https://doi.org/10.1016/j.scitotenv.2019.06.418, 2019.

Nolte, C. G., Schauer, J. J., Cass, G. R., and Simoneit, B. R. T.: Highly polar organic compounds present in wood smoke and in the ambient atmosphere, Environ. Sci. Technol., 35, 1912−1919, https://doi.org/10.1021/es001420r, 2001.

Nozière, B., Dziedzic, P., and Córdova, A.: Products and kinetics of the liquid-phase reaction of glyoxal catalyzed by ammonium ions (NH_4^+), J. Phys. Chem. A, 113, 231−237, https://doi.org/10.1021/jp8078293, 2009.

Nozière, B., Dziedzic, P., and Córdova, A.: Inorganic ammonium salts and carbonate salts are efficient catalysts for aldol condensation in atmospheric aerosols, Phys. Chem. Chem. Phys., 12, 3864−3872, https://doi.org/10.1039/B924443C, 2010.

Nozière, B., Fache, F., Maxut, A., Fenet, B., Baudouin, A., Fine, L., and Ferronato, C.: The hydrolysis of epoxides catalyzed by inorganic ammonium salts in water: kinetic evidence for hydrogen bond catalysis, Phys. Chem. Chem. Phys., 20, 1583−1590, https://doi.org/10.1039/C7CP06790A, 2018.

Pang, H., Zhang, Q., Lu, X., Li, K., Chen, H., Chen, J., Yang, X., Ma, Y., Ma, J., and Huang, C.: Nitrite-mediated photooxidation of vanillin in the atmospheric aqueous phase, Environ. Sci. Technol., 53, 14253−14263, https://doi.org/10.1021/acs.est.9b03649, 2019.

Perry, R. H., Cooks, R. G., and Noll, R. J.: Orbitrap mass spectrometry: instrumentation, ion motion and applications, Mass Spectrom. Rev., 27, 661–699, https://doi.org/10.1002/mas.20186, 2008.

Powelson, M. H., Espelien, B. M., Hawkins, L. N., Galloway, M. M., and De Haan, D. O.: Brown carbon formation by aqueous-phase carbonyl compound reactions with amines and ammonium sulfate, Environ. Sci. Technol., 48, 985−993, https://doi.org/10.1021/es4038325, 2014.

Pye, H. O. T., Nenes, A., Alexander, B., Ault, A. P., Barth, M. C., Clegg, S. L., Collett, J. L. Jr., Fahey, K. M., Hennigan, C. J., Herrmann, H., Kanakidou, M., Kelly, J. T., Ku, I., McNeill, V. F., Riemer, N., Schaefer, T., Shi, G., Tilgner, A., Walker, J. T., Wang, T., Weber, R., Xing, J., Zaveri, R. A., and Zuend, A.: The acidity of atmospheric particles and clouds, Atmos. Chem. Phys., 20, 4809–4888, https://doi.org/10.5194/acp-20-4809-2020, 2020.

Raja, S., Raghunathan, R., Yu, X., Lee, T., Chen, J., Kommalapati, R. R., Murugesan, K., Shen, X., Qingzhong, Y., Valsaraj, K. T., and Collett, J. L. Jr.: Fog chemistry in the Texas-Louisiana Gulf Coast corridor, Atmos. Environ., 42, 2048−2061, https://doi.org/10.1016/j.atmosenv.2007.12.004, 2008.

Rogge, W. F., Hildemann, L. M., Mazurek, M. A., and Cass, G. R.: Sources of fine organic aerosol. 9. Pine, oak, and synthetic log combustion in residential fireplaces, Environ. Sci. Technol., 32, 13−22, https://doi.org/10.1021/es960930b, 1998.

Romonosky, D. E., Li, Y., Shiraiwa, M., Laskin, A., Laskin, J., and Nizkorodov, S. A.: Aqueous photochemistry of secondary organic aerosol of α-Pinene and α-Humulene oxidized with ozone, hydroxyl radical, and nitrate radical, J. Phys. Chem. A, 121, 1298–1309, https://doi.org/10.1021/acs.jpca.6b10900, 2017.

Sagebiel, J. C., Seiber, J. N., and Woodrow, J. E.: Comparison of headspace and gas-stripping methods for determining the Henry's law constant (H) for organic compounds of low to intermediate H, Chemosphere, 25, 1763–1768, https://doi.org/10.1016/0045-6535(92)90017-L, 1992.

Schauer, J. J., Kleeman, M. J., Cass, G. R., and Simoneit, B. R. T.: Measurement of emissions from air pollution sources. 3. C_1-C_{29} organic compounds from fireplace combustion of wood, Environ. Sci. Technol., 35, 1716−1728, https://doi.org/10.1021/es001331e, 2001.

Schmidt, A-C., Herzschuh, R., Matysik, F-M., and Engewald, W.: Investigation of the ionisation and fragmentation behaviour of different nitroaromatic compounds occurring as polar metabolites of explosives using electrospray ionisation tandem mass spectrometry, Rapid Commun. Mass Sp., 20, 2293–2302, https://doi.org/10.1002/rcm.2591, 2006.

Shapiro, E. L., Szprengiel, J., Sareen, N., Jen, C. N., Giordano, M. R., and McNeill, V. F.: Light-absorbing secondary organic material formed by glyoxal in aqueous aerosol mimics, Atmos. Chem. Phys., 9, 2289−2300, https://doi.org/10.5194/acp-9-2289-2009, 2009.

777

778 Siegmann, K. and Sattler, K.: Formation mechanism for polycyclic aromatic hydrocarbons in methane flames, J. Chem.
779 Phys., 112, 698–709, https://doi.org/10.1063/1.480648, 2000.

780

781 Simoneit, B. R. T.: Biomass burning — a review of organic tracers for smoke from incomplete combustion, Appl.
782 Geochem., 17, 129–162, https://doi.org/10.1016/S0883-2927(01)00061-0, 2002.

783

784 Simoneit, B. R. T., Rogge, W. F., Mazurek, M. A., Standley, L. J., Hildemann, L. M., and Cass, G. R.: Lignin pyrolysis
785 products, lignans, and resin acids as specific tracers of plant classes in emissions from biomass combustion, Environ. Sci.
786 Technol., 27, 2533−2541, https://doi.org/10.1021/es00048a034, 1993.

787

788 Simoneit, B. R. T., Schauer, J. J., Nolte, C. G., Oros, D. R., Elias, V. O., Fraser, M. P., Rogge, W. F., and Cass, G. R.:
789 Levoglucosan, a tracer for cellulose in biomass burning and atmospheric particles, Atmos. Environ., 33, 173−182,
790 https://doi.org/10.1016/S1352-2310(98)00145-9, 1999.

791

792 Simpson, C. D., Paulsen, M., Dills, R. L., Liu, L.-J. S., and Kalman, D. A.: Determination of methoxyphenols in ambient
793 atmospheric particulate matter: tracers for wood combustion, Environ. Sci. Technol., 39, 631−637,
794 https://doi.org/10.1021/es0486871, 2005.

795

796 Slikboer, S., Grandy, L., Blair, S. L., Nizkorodov, S. A., Smith, R. W., and Al-Abadleh, H. A.: Formation of light absorbing
797 soluble secondary organics and insoluble polymeric particles from the dark reaction of catechol and guaiacol with Fe(III),
798 Environ. Sci. Technol., 49, 7793–7801, https://doi.org/10.1021/acs.est.5b01032, 2015.

799

800 Smith, D. F., Kleindienst, T. E., and McIver, C. D.: Primary product distributions from the reaction of OH with m-, p-xylene,
801 1,2,4-and 1,3,5-trimethylbenzene, J. Atmos. Chem., 34, 339–364, https://doi.org/10.1023/A:1006277328628, 1999.

802

803 Smith, J. D., Sio, V., Yu, L., Zhang, Q., and Anastasio, C.: Secondary organic aerosol production from aqueous reactions of
804 atmospheric phenols with an organic triplet excited state, Environ. Sci. Technol., 48, 1049–1057,
805 https://doi.org/10.1021/es4045715, 2014.

806

807 Smith, J. D., Kinney, H., and Anastasio, C.: Aqueous benzene-diols react with an organic triplet excited state and hydroxyl
808 radical to form secondary organic aerosol, Phys. Chem. Chem. Phys., 17, 10227−10237,
809 https://doi.org/10.1039/C4CP06095D, 2015.

810

811 Smith, J. D., Kinney, H., and Anastasio, C.: Phenolic carbonyls undergo rapid aqueous photodegradation to form low-
812 volatility, light-absorbing products, Atmos. Environ., 126, 36−44, https://doi.org/10.1016/j.atmosenv.2015.11.035, 2016.

813

814 Song, J., Li, M., Jiang, B., Wei, S., Fan, X., and Peng, P.: Molecular characterization of water-soluble humic like substances
815 in smoke particles emitted from combustion of biomass materials and coal using ultrahigh-resolution electrospray ionization
816 Fourier transform ion cyclotron resonance mass spectrometry, Environ. Sci. Technol., 52, 2575–2585,
817 https://doi.org/10.1021/acs.est.7b06126, 2018.

818

819 Sun, Y. L., Zhang, Q., Anastasio, C., and Sun, J.: Insights into secondary organic aerosol formed via aqueous-phase
820 reactions of phenolic compounds based on high resolution mass spectrometry, Atmos. Chem. Phys., 10, 4809−4822,
821 https://doi.org/10.5194/acp-10-4809-2010, 2010.

822

823 US EPA: Estimation Programs Interface Suite™ for Microsoft® Windows, v 4.1, United States Environmental Protection
824 Agency, Washington, DC, USA, 2012.

825

Wang, K., Huang, R-J., Brüggemann, M., Zhang, Y., Yang, L., Ni, H., Guo, J., Wang, M., Han, J., Bilde, M., Glasius, M., and Hoffmann, T.: Urban organic aerosol composition in eastern China differs from north to south: molecular insight from a liquid chromatography–mass spectrometry (Orbitrap) study, Atmos. Chem. Phys., 21, 9089–9104, https://doi.org/10.5194/acp-21-9089-2021, 2021.

Wang, X., Hayeck, N., Brüggemann, M., Yao, L., Chen, H., Zhang, C., Emmelin, C., Chen, J., George, C., and Wang, L.: Chemical characterization of organic aerosols in Shanghai: A study by ultrahigh-performance liquid chromatography coupled with orbitrap mass spectrometry, J. Geophys. Res. Atmos., 122, 11703–11722, https://doi.org/10.1002/2017JD026930, 2017.

Wang, Y., Huang, D. D., Huang, W., Liu, B., Chen, Q., Huang, R., Gen, M., Mabato, B. R. G., Chan, C. K., Li, X., Hao, T., Tan, Y., Hoi, K. I., Mok, K. M., and Li, Y. J.: Enhanced nitrite production from the aqueous photolysis of nitrate in the presence of vanillic acid and implications for the roles of light-absorbing organics, Environ. Sci. Technol., 55, 15694−15704, https://doi.org/10.1021/acs.est.1c04642, 2021.

Wang, Y., Huang, W., Tian, L., Wang, Y., Li, F., Huang, D. D., Zhang, R., Mabato, B. R. G., Huang, R., Chen, Q., Ge, X., Du, L., Ma, Y. G., Gen, M., Hoi, K. I., Mok, K. M., Yu, J. Z., Chan, C. K., Li, X., and Li, Y. J.: Decay kinetics and absorption changes of methoxyphenols and nitrophenols during nitrate-mediated aqueous photochemical oxidation at 254 and 313 nm, ACS Earth Space Chem., 6, 1115−1125, https://doi.org/10.1021/acsearthspacechem.2c00021, 2022.

Yang, J., Au, W. C., Law, H., Leung, C. H., Lam, C. H, and Nah, T.: pH affects the aqueous-phase nitrate-mediated photooxidation of phenolic compounds: implications for brown carbon formation and evolution, Environ. Sci.: Processes Impacts, https://doi.org/10.1039/D2EM00004K, 2022.

Yasmeen, F., Vermeylen, R., Szmigielski, R., Iinuma, Y., Böge, O., Herrmann, H., Maenhaut, W., and Claeys, M.: Terpenylic acid and related compounds: precursors for dimers in secondary organic aerosol from the ozonolysis of α and β-pinene, Atmos. Chem. Phys., 10, 9383–9392, https://doi.org/10.5194/acp-10-9383-2010, 2010.

Yaws, C. L.: Handbook of vapor pressure, volume 3: Organic compounds C8 to C28, Gulf Professional Publishing, 1994.

Ye, Z., Qu, Z., Ma, S., Luo, S., Chen, Y., Chen, H., Chen, Y., Zhao, Z., Chen, M., and Ge, X.: A comprehensive investigation of aqueous-phase photochemical oxidation of 4-ethylphenol, Sci. Total Environ., 685, 976–985, https://doi.org/10.1016/j.scitotenv.2019.06.276, 2019.

Yu, G., Bayer, A. R., Galloway, M. M., Korshavn, K. J., Fry, C. G., and Keutsch, F. N.: Glyoxal in aqueous ammonium sulfate solutions: products, kinetics and hydration effects, Environ. Sci. Technol., 45, 6336−6342, https://doi.org/10.1021/es200989n, 2011.

Yu, L., Smith, J., Laskin, A., Anastasio, C., Laskin, J., and Zhang, Q.: Chemical characterization of SOA formed from aqueous-phase reactions of phenols with the triplet excited state of carbonyl and hydroxyl radical, Atmos. Chem. Phys., 14, 13801−13816, https://doi.org/10.5194/acp-14-13801-2014, 2014.

Yu, L., Smith, J., Laskin, A., George, K. M., Anastasio, C., Laskin, J., Dillner, A. M., and Zhang, Q.: Molecular transformations of phenolic SOA during photochemical aging in the aqueous phase: competition among oligomerization, functionalization, and fragmentation, Atmos. Chem. Phys., 16, 4511−4527, https://doi.org/10.5194/acp-16-4511-2016.

Zhang, Q. and Anastasio, C.: Conversion of fogwater and aerosol organic nitrogen to ammonium, nitrate, and NO$_x$ during exposure to simulated sunlight and ozone, Environ. Sci. Technol., 37, 3522–3530, https://doi.org/10.1021/es034114x, 2003.

Zhang, R., Gen, M., Huang, D. D., Li, Y. J., and Chan, C. K.: Enhanced sulfate production by nitrate photolysis in the presence of halide ions in atmospheric particles, Environ. Sci. Technol., 54, 3831–3839, https://doi.org/10.1021/acs.est.9b06445, 2020.

Zhang, R., Gen, M., Fu, T-M., and Chan, C. K.: Production of formate via oxidation of glyoxal promoted by particulate nitrate photolysis, Environ. Sci. Technol., 55, 5711–5720, https://doi.org/10.1021/acs.est.0c0819, 2021.

Zhang, R., Gen, M., Liang, Z., Li, Y. J., and Chan, C. K.: Photochemical reactions of glyoxal during particulate ammonium nitrate photolysis: Brown carbon formation, enhanced glyoxal decay, and organic phase formation, Environ. Sci. Technol., 56, 1605–1614, https://doi.org/10.1021/acs.est.1c07211, 2022.

Zielinski, T., Bolzacchini, E., Cataldi, M., Ferrero, L., Graßl, S., Hansen, G., Mateos, D., Mazzola, M., Neuber, R., Pakszys, P., Posyniak, M., Ritter, C., Severi, M., Sobolewski, P., Traversi, R., and Velasco-Merino, C.: Study of chemical and optical properties of biomass burning aerosols during long-range transport events toward the Arctic in summer 2017, Atmosphere, 11, 84, https://doi.org/10.3390/atmos11010084, 2020.

Table 1. Reaction conditions, initial GUA (and DMB or VL) decay rate constants, normalized abundance of products, average elemental ratios, and average carbon oxidation state ($\langle OS_C \rangle$) in each experiment. The reaction systems consisted of GUA (0.1 mM), DMB (0.01 mM), VL (0.01 mM), and AN (1 mM) under air-saturated conditions after 180 min of simulated sunlight irradiation. The UHPLC-HESI-Orbitrap-MS data were obtained in both positive (POS) and negative (NEG) ion modes.

Exp no.	Reaction conditions	Initial GUA (and DMB or VL) decay rate constants (min⁻¹/s⁻¹)[a]	Normalized abundance of products[b]	Normalized abundance of N-containing compounds[b]	$\langle O:C \rangle$[c]	$\langle H:C \rangle$[c]	$\langle N:C \rangle$[c]	$\langle OS_C \rangle$[c]
1	GUA+DMB	GUA: ~~5.4 × 10⁻²~~6.3 ± 0.25~~3.0 × 10⁻⁴~~ DMB: 0.~~6.7 × 10⁻³~~78 ± 0~~1~~.10~~2 × 10⁻⁴~~	376 ± 22	NA	POS: 0.34	0.91	NA	-0.22
					NEG: 0.40	0.94	NA	-0.15
2	GUA+ DMB+AN	GUA: ~~4.8 × 10⁻²~~ 5.3 ± 0~~6.5~~~~04 × 10⁻⁴~~ DMB: ~~6.2 × 10⁻³~~0.69 ± -0.05~~6.25 × 10⁻⁵~~	310 ± 4	114	POS: 0.28	0.94	0.12	-0.03
					NEG: 0.37	0.91	0.04	-0.05
3	GUA+VL	GUA: ~~1.4 × 10⁻²~~1.5 ± 0~~1~~.1~~48 × 10⁻⁴~~ VL: ~~3.3 × 10⁻²~~3.6 ± 0.55~~7.0 × 10⁻⁴~~	94 ± 5	NA	POS: 0.41	0.91	NA	-0.10
					NEG: 0.40	0.94	NA	-0.14
~~3~~4	GUA+ VL+AN	GUA: ~~1.5 × 10⁻²~~1.6 ± 0.1~~26 × 10⁻⁴~~ VL: ~~2.8 × 10⁻²~~2.9 ± 0.032~~4.9 × 10⁻⁵~~	100 ± 2	8	POS: 0.31	1.02	0.02	-0.34
					NEG: 0.39	0.91	0.03	-0.02
5	GUA+AN	~~8.1 × 10⁻³~~ 0.57 ± 0.03~~7.62 × 10⁻⁵~~	23 ± 1	9	POS: 0.35	0.99	0.16	0.19
					NEG: 0.38	1.01	0.05	-0.08

[a]The data fitting was performed in the initial linear region. Each value is the average of results from triplicate experiments, corrected for internal light screening due to DMB, VL, and AN, and normalized to the experimental photon flux. Errors represent one standard deviation. [b]The normalized product abundance was calculated using the data from UHPLC-HESI-Orbitrap-MS in the positive (POS) ion mode as the GUA signal from the negative (NEG) ion mode was weak, which may introduce significant uncertainties during normalization. The uncertainties were propagated from the changes in [GUA] measured using UHPLC-PDA and the MS signal intensities. The samples for experiments without AN (marked with NA) were not analyzed for N-containing compounds. [c]The average elemental ratios ($\langle O:C \rangle$, $\langle H:C \rangle$, and $\langle N:C \rangle$) and $\langle OS_C \rangle$ were

929 based on the UHPLC-HESI-Orbitrap-MS results and estimated using the signal-weighted method (Bateman et al., 2012).

930 The $\langle OS_C \rangle$ of GUA, DMB, and VL are -0.57, -0.44, and -0.25, respectively.

931
932
933
934
935
936
937
938
939
940
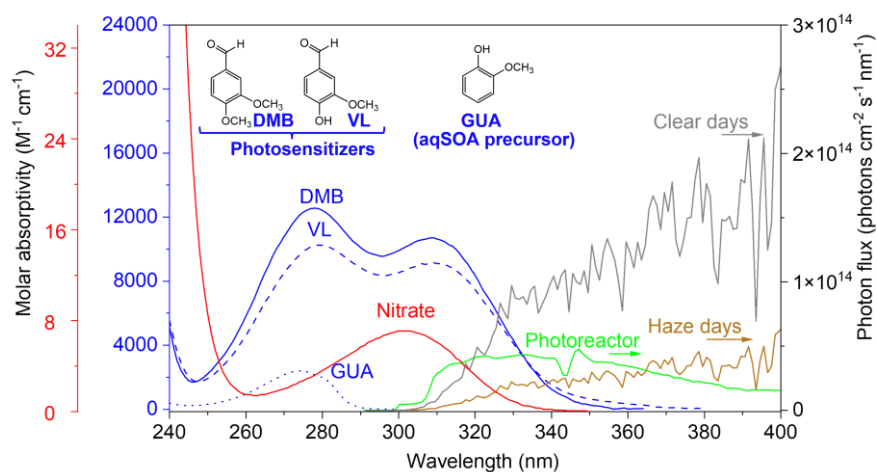
949 **Figure 1.** The base-10 molar absorptivities (M^{-1} cm^{-1}) of 3,4-dimethoxybenzaldehyde (DMB, blue solid line), vanillin (VL, blue dashed line), guaiacol (GUA, blue dotted line), and nitrate (red solid line). The green line is the photon flux in the aqueous photoreactor. The gray and brown lines are the photon fluxes on typical clear and~~or~~ haze days, respectively, in Beijing, China (Mabato et al., 2022). The top of the figure also shows the structures of DMB, VL, and GUA.
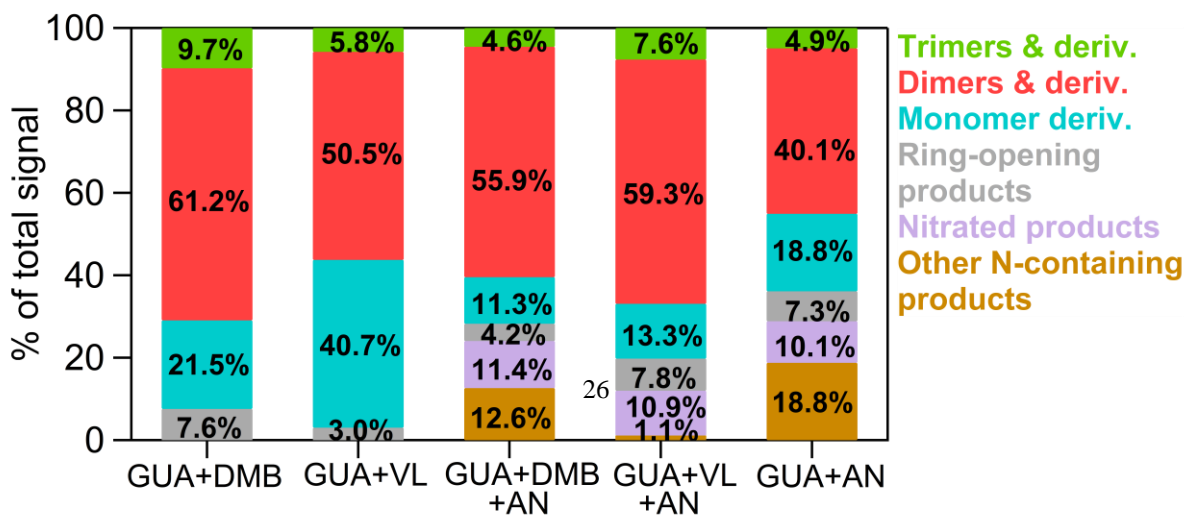
953 **Figure 2.** Signal-weighted distributions of aqSOA from GUA+DMB, GUA+VL, GUA+DMB+AN, GUA+VL+AN, and

954 GUA+AN. These product distributions were calculated from combined UHPLC-HESI-Orbitrap-MS data obtained in positive

955 (POS) and negative (NEG) ion modes. The values indicate the contribution of different product classifications to the total

956 signals for each reaction condition.

957
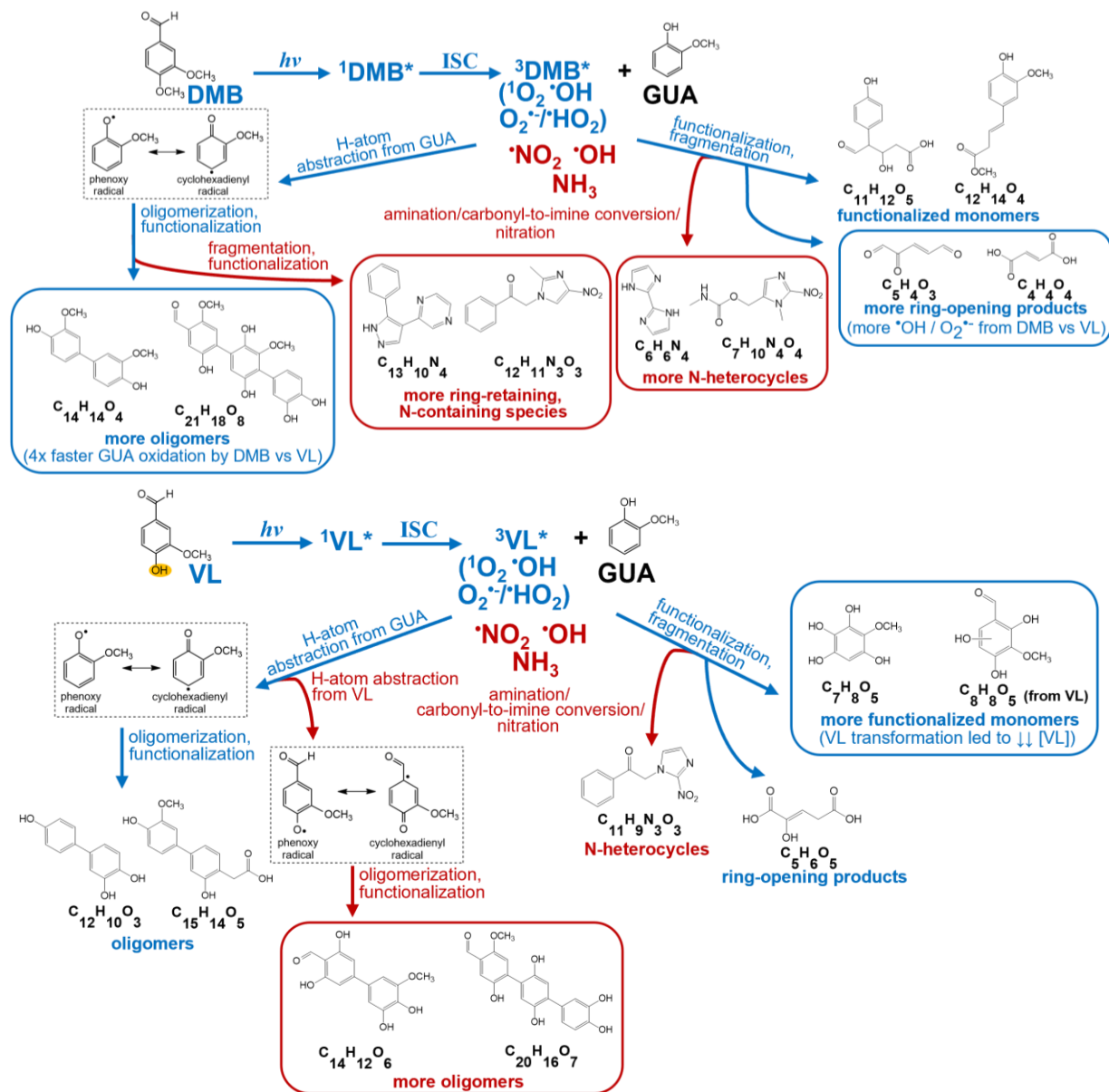
Figure 3. Summary of the main differences between photosensitized GUA oxidation by ^{3}DMB* (top) and ^{3}VL* (bottom) in the absence (blue labels and boxes) and presence (red labels and boxes) of ammonium nitrate at pH 4 under air-saturated conditions. Boxed structures indicate product classifications with notable differences. DMB and VL absorb light and are promoted to their singlet excited states (^{1}DMB* and ^{1}VL*), which then undergo intersystem crossing (ISC) to form ^{3}DMB* and ^{3}VL*. Secondary oxidants (^{1}O$_2$, O$_2^{\bullet-}$/$^{\bullet}$HO$_2$, $^{\bullet}$OH) can be formed from ^{3}DMB* and ^{3}VL* upon reactions with O$_2$ and GUA (George et al., 2018; Chen et al., 2020; Misovich et al., 2021; Mabato et al., 2022). The structures shown are examples of the major products (Tables S1 to S4) for different product classifications.
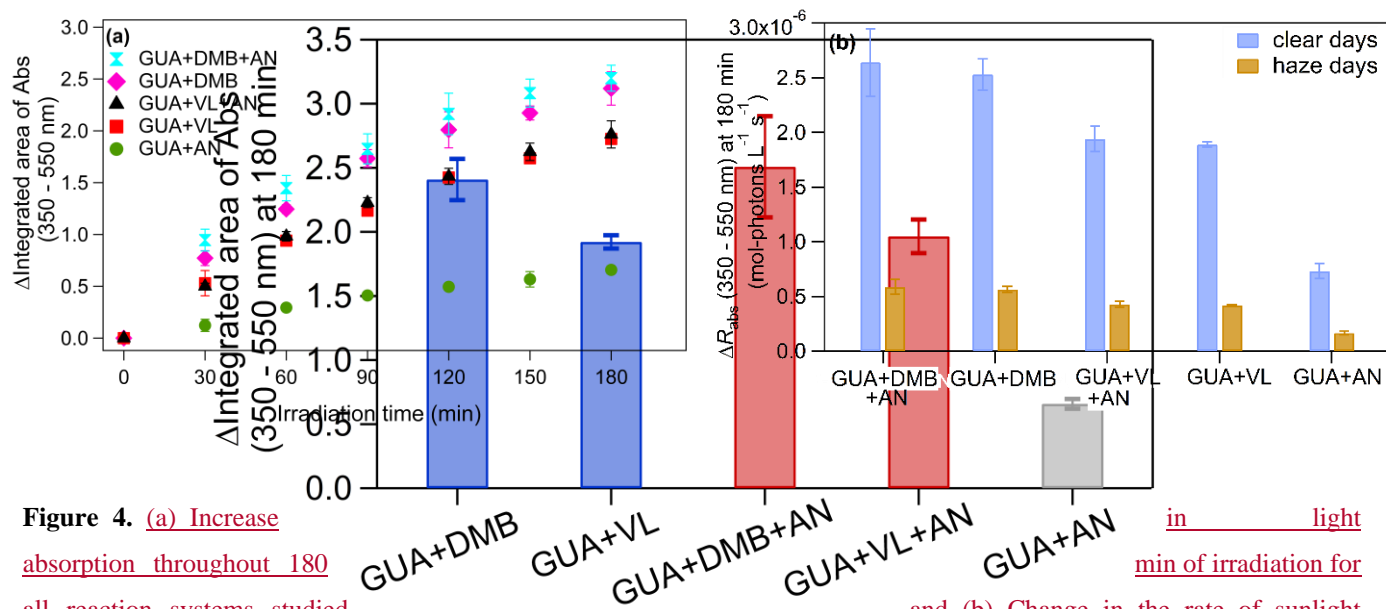
Figure 4. (a) Increase absorption throughout 180 min of irradiation for all reaction systems studied and (b) Change in the rate of sunlight absorption (ΔR_{abs}) from 350-550 nm at 180 min during typical clear and haze days in Beijing, China for aqSOA from GUA+DMB+AN, GUA+DMB, GUA+VL+AN, GUA+VL, and GUA+AN. ~~Increase in visible light absorption for aqSOA from GUA+DMB, GUA+VL, GUA+DMB+AN, and GUA+VL+AN.~~ Error bars represent one standard deviation of triplicate experiments.

29

1 **Supplementary material**

2

3 **Comparison of a~~A~~**queous SOA **product distributions**
4 ~~formation~~ from ~~photosensitized~~ guaiacol oxidation **by~~:~~**
5 ~~Comparison between~~ **non-phenolic and phenolic**
6 **methoxybenzaldehydes as photosensitizers in the absence and**
7 **presence of ammonium nitrate**

8

9 Beatrix Rosette Go Mabato[1,2], Yong Jie Li[3], Dan Dan Huang[4], Yalin Wang[3], and Chak K.
10 Chan[1,2]*

11

12 [1]School of Energy and Environment, City University of Hong Kong, Hong Kong, China

13 [2]City University of Hong Kong Shenzhen Research Institute, Shenzhen, China

14 [3]Department of Civil and Environmental Engineering, and Centre for Regional Ocean,

15 Faculty of Science and Technology, University of Macau, Macau, China

16 [4]Shanghai Academy of Environmental Sciences, Shanghai 200233, China

17

18
19
20

21 *Correspondence to*: Chak K. Chan (Chak.K.Chan@cityu.edu.hk)

22
23
24
25
26
27
28
29
30
31

Section S1. UHPLC-PDA analyses

An ultra-high performance liquid chromatography system (UHPLC, Waters Acquity H-Class, Waters, Milford, USA) coupled to a photodiode array (PDA) detector (Waters, Milford, USA) was used for the quantification of GUA, DMB, and VL concentrations. The samples were first filtered through a 0.2 μm Chromafil® Xtra PTFE filter (Macherey-Nagel GmbH & Co. KG, Germany). The separation of products was conducted using an Acquity HSS T3 column (1.8 μm, 2.1 mm × 100 mm; Waters Corp.). The column oven was held at 30 °C, and the autosampler was cooled at 4 °C. The injection volume was set to 5 μL. The binary mobile phase was composed of water (A) and acetonitrile (B). The gradient elution was performed at a flow rate of 0.2 mL/min: 0–1 min, 10% eluent B; 1–25 min, linear increase to 90% eluent B; 25–29.9 min, hold 90% eluent B; 29.9–30 min, decrease to 10% eluent B; 30–35 min, re-equilibrate at 10% eluent B for 5 min. GUA, DMB, and VL were analyzed using the channels with UV absorption at 274, 274, and 300 nm, respectively.

Section S2. UHPLC-HESI-Orbitrap-MS analyses

A Thermo Orbitrap Fusion Lumos Mass Spectrometry (Thermo Fisher Scientific, Waltham, MA, USA) connected to a Thermo Scientific UltiMate 3000 UHPLC system (Thermo Fisher Scientific, Waltham, MA, USA) via heated electrospray ionization (HESI) as the interface (UHPLC-HESI-Orbitrap-MS) was used to characterize the reaction products. The mobile phases used were 0.1% (v/v) formic acid (in milli-Q water) (A) and acetonitrile (B). The same settings (e.g., column, gradient, oven temperature) used in the UHPLC-PDA (Sect. S1) were applied in the UHPLC-HESI-Orbitrap-MS system. The HESI-MS spectra were acquired in both positive and negative ion modes. The HESI parameters were as follows: Spray voltage, 2500 V for both positive and negative HESI; sheath gas, 35 arbitrary units; nebulizer auxiliary gas, 10 arbitrary units; sweep gas, 3 arbitrary units. General instrumental parameters were set as follows: ion transfer tube temperature, 320 °C; vaporizer temperature, 350 °C. The mass

58   range for full scan MS was set at 50-1000 m/z with a mass resolution of 60,000 at 200 m/z.

59   The automatic gain control (AGC) target was 4.0×10^5 with a maximum injection time of 50

60   ms. The UHPLC-HESI-Orbitrap-MS data obtained in positive and negative ion modes were

61   pretreated using Progenesis QI (version 2.4; Nonlinear Dynamics) for peak picking and

62   alignment. Most peaks detected in the blank (~99% for all experiments) were excluded from

63   the samples except for peaks with a minimum of 2.5 times greater intensity in the sample

64   spectrum than in the blank (Laskin et al., 2014). In addition, a peak was considered a product

65   if the difference in the peak area between the samples before and after irradiation is ≥10 times.

66   In this work, two independently prepared samples for each reaction condition were analyzed

67   using the UHPLC-HESI-Orbitrap-MS. Only peaks that were reproducibly detected in both sets

68   of samples were retained. The formula assignments were carried out using the MIDAS

69   molecular formula calculator (http://magnet.fsu.edu/~midas/) with the following constraints: C

70   ≤100, H ≤150, O ≤30, and N ≤10, and mass error of 10 ppm. The nitrogen atom was excluded

71   in the constraints for experiments without AN. The ChemSpider database (Royal Society of

72   Chemistry) was also queried to return valid molecules that may be useful for proposing product

73   structures. Overall, the proposed structures in this work are based on the molecular formulas,

74   DBE values, and structural and mechanistic information provided in earlier similar works on

75   methoxyphenols (Yee et al., 2013; Li et al., 2014; Yu et al., 2014, 2016; He et al., 2019; Chen

76   et al., 2020; Jiang et al., 2021; Misovich et al., 2021; Mabato et al., 2022). For clarity, the

77   formulas discussed in this work correspond to neutral analytes (e.g., with H^+ or NH_4^+ removed

78   from the ion formula).

79   The double bond equivalent (DBE) values (Koch and Dittmar, 2006) and carbon

80   oxidation state (OS_C; Kroll et al., 2011, 2015; Lv et al., 2016) of the neutral formulas were

81   calculated using the following equations:

82

83 $$DBE = C - H/2 + N/2 + 1 \qquad \text{(Eq. S1)}$$

84 $$OS_C = 2 \times O/C + 3 \times N/C - H/C \qquad \text{(Eq. S2)}$$

85 where C, H, O, and N correspond to the number of carbon, hydrogen, oxygen, and nitrogen

86 atoms in the neutral formula. Moreover, the average oxygen to carbon (O:C) ratios, $\langle$O:C$\rangle$:

87 ($\langle O: C \rangle = \sum_i (\text{abundance}_i) O_i / \sum_i (\text{abundance}_i) C_i$), average nitrogen to carbon (N:C) ratios,

88 $\langle$N:C$\rangle$: ($\langle N: C \rangle = \sum_i (\text{abundance}_i) N_i / \sum_i (\text{abundance}_i) C_i$), and average hydrogen to carbon

89 (H:C) ratios, $\langle$H:C$\rangle$: ($\langle H: C \rangle = \sum_i (\text{abundance}_i) H_i / \sum_i (\text{abundance}_i) C_i$) after the reactions

90 were further estimated using the signal-weighted method (Bateman et al., 2012). The average

91 OS_C, $\langle OS_C \rangle$ was also calculated as follows:

92 $$\langle OS_C \rangle = 2 \times \langle O:C \rangle + 3 \times \langle N:C \rangle - \langle H:C \rangle \qquad \text{(Eq. S3)}$$

93 **Section S3. IC analyses of small organic acids**

94 An ion chromatography system (IC, Dionex ICS-1100, Sunnyvale, CA) equipped with a

95 Dionex AS-DV autosampler (Sunnyvale, CA) enabled the analyses of small organic acids. The

96 separation was achieved using an IonPac$^{\text{TM}}$ AS11 column (4×250 mm) with an IonPac$^{\text{TM}}$

97 AG11 guard column (4×50 mm). The isocratic elution was applied at a 1.0 mL/min flow rate

98 with 12 mM sodium hydroxide (NaOH) as the eluent. The total run time was set at 10 min. The

99 standard solutions (1–50 μM) of formic, succinic, and oxalic acid were analyzed three times

100 along with the samples and water blank. Formic, succinic, and oxalic acid had retention times

101 of 1.9 min, 3.7 min, and 5.9 min, respectively.

102 **Section S4. UV-Vis spectrophotometric analyses**

103 A UV-Vis spectrophotometer (UV-3600, Shimadzu Corp., Japan) was used to measure the

104 absorbance changes for the samples. The absorbance values from 200 to 700 nm were measured

105 instantly after sample collection, and measurements were done in triplicate. The change in the

106 integrated area of absorbance from 350 to 550 nm was used to represent the absorbance

107 enhancements. The increase of light absorption at this wavelength range, where GUA, DMB,

108 and VL did not initially absorb light, suggests the formation of light-absorbing products (Smith

109 et al., 2016).

110 **Section S5. Further discussions on van Krevelen diagrams and OS_c vs. n_C plots for**

111 **GUA+DMB and GUA+VL aqSOA**

112 Consistent with the higher contribution of ring-opening species, GUA+DMB had more

113 products with H:C ≥1.5 and O:C ≤0.5 (Fig. S54a–b), possibly due to more oxygenated aliphatic

114 species. GUA+VL (Fig. S54c–d) also had high-relative-abundance products with H:C of ~1

115 and O:C ≥0.5. Similar to our previous work (0.1 mM GUA + 0.1 mM VL; Mabato et al., 2022),

116 the two high-relative-abundance species with O:C ≥0.5 were associated with hydroxylated

117 products ($C_7H_8O_4$ and $C_8H_8O_5$, #28 and 35; Table S2) that were also observed in earlier works

118 on $^3DMB^*$ and $^\bullet OH$-mediated oxidation (Yu et al., 2014, 2016). These hydroxylated products

119 were also present in GUA+DMB but with lower relative abundance. Triplet-mediated phenol

120 oxidation can generate H_2O_2 (Anastasio et al., 1997), a photolytic source of $^\bullet OH$. Indeed,

121 hydroxylation is significant in aqueous-phase phenol oxidation (Li et al., 2014; Yu et al., 2014,

122 2016; Chen et al., 2020; Jiang et al., 2021; Misovich et al., 2021; Mabato et al., 2022).

123   The OS_C vs. n_C plots for both GUA+DMB and GUA+VL display high-relative-

124 abundance species clustered at n_C of 12 to 15 and OS_C >-1, which can be ascribed to dimers

125 and derivatives (Fig. S65a–d). The species with n_C >15 had the highest DBE values and can be

126 attributed to trimers. These compounds were more abundant in GUA+DMB, likely due to the

127 greater extent of photosensitized reactions by $^3DMB^*$ compared to $^3VL^*$. Indeed,

128 oligomerization is an important process in aqSOA formation via triplet-mediated oxidation (Yu

129 et al., 2014, 2016; Chen et al., 2020; Jiang et al., 2021; Misovich et al., 2021; Mabato et al.,

130 2022). As indicated by the higher quantity of low DBE species, ring-opening and fragmentation

131 pathways were more extensive in GUA+DMB. In GUA+VL, there were also high-relative-

132   abundance products with n_C <10, OS_C ≥0, and DBE <5, corresponding to the hydroxylated

133   products mentioned earlier.

Section S6. Estimation of the apparent quantum efficiency of guaiacol photodegradation

135   The apparent quantum efficiency of GUA photodegradation (φ_{GUA}) in the presence of DMB,

136   VL, or nitrate during simulated sunlight illumination can be defined as (Anastasio et al., 1997;

137   Smith et al., 2014, 2016):

138    $$\Phi_{GUA} = \frac{\text{mol GUA destroyed}}{\text{mol photons absorbed}} \qquad \text{(Eq. S4)}$$

139   Φ_{GUA} was calculated using the measured rate of GUA decay and rate of light absorption by

140   DMB, VL, or nitrate through the following equation:

141    $$\Phi_{GUA} = \frac{\text{rate of GUA decay}}{\text{rate of light absorption by DMB or VL or nitrate}} = \frac{k'_{GUA} \times [GUA]}{\sum[(1-10^{-\varepsilon_\lambda[C]l}) \times I'_\lambda]} \qquad \text{(Eq. S5)}$$

142   where k'_{GUA} is the pseudo-first-order rate constant for GUA decay, [GUA] is the concentration

143   of GUA (M), ε_λ is the base-10 molar absorptivity (M^{-1} cm^{-1}) of DMB, VL, or nitrate at

144   wavelength λ, [C] is the concentration of DMB, VL, or nitrate (M), l is the pathlength of the

145   illumination cell (cm), and I'_λ is the volume-averaged photon flux (mol-photons L^{-1} s^{-1} nm^{-1})

146   determined from 2NB actinometry:

147    $$j(2NB) = 2.303 \times \Phi_{2NB} \times l \times \Sigma_{300\,nm}^{350\,nm}(\varepsilon_{2NB,\lambda} \times I'_\lambda \times \Delta\lambda) \qquad \text{(Eq. S6)}$$

148   where $j(2NB)$ is the decay rate constant of 2-nitrobenzaldehyde (2NB), the chemical

149   actinometer used to determine the photon flux in the aqueous photoreactor, $\Phi_{2NB,\lambda}$ and $\varepsilon_{2NB,\lambda}$

150   are the quantum yield (molecule $photon^{-1}$) and base-10 molar absorptivity (M^{-1} cm^{-1}) for 2NB,

151   respectively, and $\Delta\lambda$ is the wavelength interval between actinic flux data points (nm).

Section S7. Further discussions on van Krevelen diagrams and OS_c vs. n_C plots for

153   **GUA+DMB+AN, GUA+VL+AN, and GUA+AN aqSOA**

154   The position of the CHO, CHON, and CHN species in the van Krevelen diagrams for

155   GUA+DMB+AN and GUA+VL+AN broadly resembled those of CHO species in the absence

of AN (Fig. S5). The CHON species for GUA+DMB+AN and GUA+VL+AN mostly had

O:C ratios <0.7, consistent with previous studies on BBOA e.g., wheat straw burning in K-

Puszta in the Great Hungarian Plain of Hungary, biomass burning at Canadian rural sites such

as Saint Anicet, and BBOA from Amazonia (Schmitt-Kopplin et al., 2010; Claeys et al., 2012;

Kourtchev et al., 2017).

The CHN species in GUA+DMB+AN and GUA+VL+AN appeared to have analogous

H:C ratios. GUA+DMB+AN had ~2 times more CHON and CHN species than GUA+VL+AN,

and there were more of these species with higher abundance in the former, indicating a greater

extent of reactions with AN. The high-relative-abundance products for GUA+DMB+AN and

GUA+VL+AN were similar to those in the absence of AN, except the hydroxylated products

(e.g., $C_7H_8O_4$; #28; Table S2) previously mentioned for GUA+VL. Among the high-relative-

abundance products for GUA+DMB+AN was a CHN species with H:C of ~0.8. For

GUA+VL+AN, the high-relative-abundance products include two CHON species with O:C

and H:C ratios of 0.3-0.6 and 0.6-0.8. The major difference between GUA+AN and

GUA+DMB+AN/GUA+VL+AN was the presence of more high-relative-abundance CHON

and CHN species (Fig. S9) in GUA+AN which can be expected given that AN was the only

source of oxidants in this case. Compared to GUA+AN, more species (CHO, CHON, and

CHN) were observed for GUA+DMB+AN and GUA+VL+AN, attributable to contributions

from both photosensitization and (ammonium) nitrate photolysis.

Moreover, GUA+DMB+AN and GUA+VL+AN aqSOA had mainly similar features in

the OS_C vs. n_C plots as those observed in the absence of AN (Fig. S6). GUA+DMB+AN and

GUA+VL+AN aqSOA also had more CHON and CHN species with higher OS_C, n_C, and DBE

(Fig. S6e–h) relative to GUA+AN (Fig. S10), indicating more conjugated N-containing

compounds. For GUA+DMB+AN and GUA+VL+AN, the CHON and CHN species had a

wider range of OS_C compared to CHO species (Fig. S6e–h). The high-relative-abundance

181   species (n_C of 12 to 15 and OS_C >-1) corresponded to dimers and trimers similar to those noted

182   in the absence of AN, along with some N-containing species. These include a CHN species

183   with n_C of 13, OS_C ~0, and 11 DBE for GUA+DMB+AN, and 2 CHON species with n_C of 5

184   and 11, OS_C of 2.5 and 1, and 6 and 9 DBE for GUA+VL+AN.

185

186

187
188
189
190
191
192
193
194
195
196
197
198
199
200
201
202
203
204
205
206
207
208
209
210
211
212
213
214
215
216
217
218
219
220
221
222
223
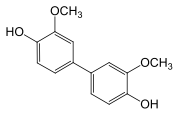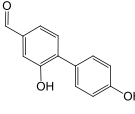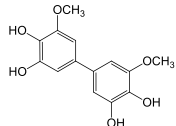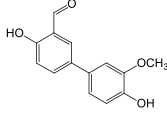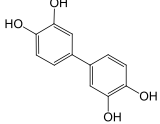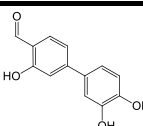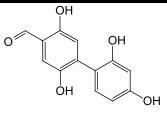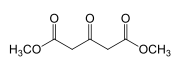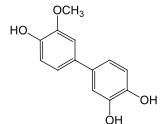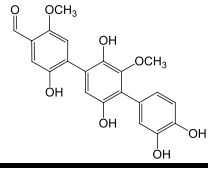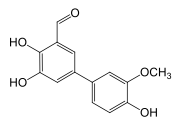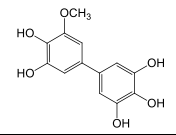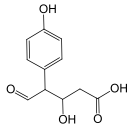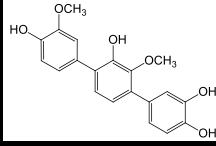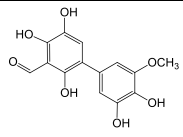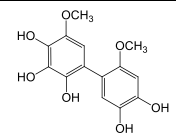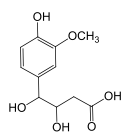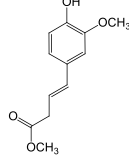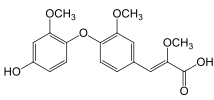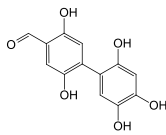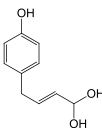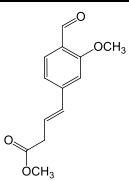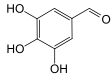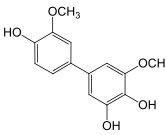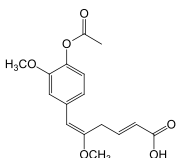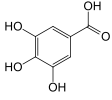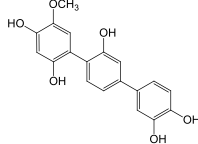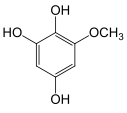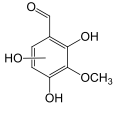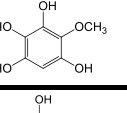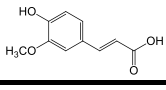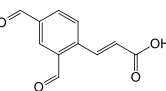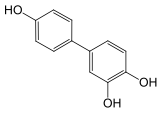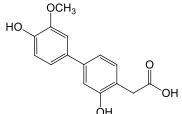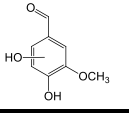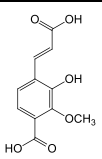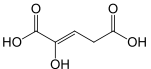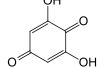
Table S1. Possible structures of the major products detected from GUA+DMB using UHPLC-HESI-Orbitrap-MS operated in positive (POS) and negative (NEG) ion modes.

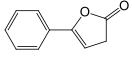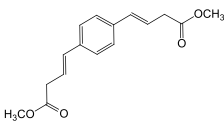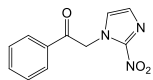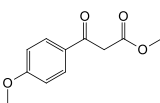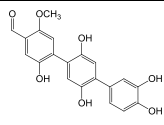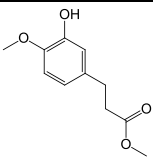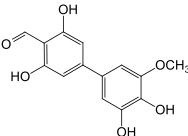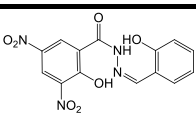| No.	GUA+DMB POS Molecular formula and exact mass	DBE	Possible structure	No.	GUA+DMB NEG Molecular formula and exact mass	DBE	Possible structure
1	$C_{14}H_{14}O_4$ (246.0892)	8			$C_{14}H_{14}O_4$ (246.0892) (No. 1; GUA+DMB POS)		
2	$C_{13}H_{10}O_3$ (214.0630)	9		16	$C_{14}H_{14}O_6$ (278.0790)	8	
3	$C_{14}H_{12}O_4$ (244.0736)	9		17	$C_{12}H_{10}O_4$ (218.0579)	8	
4	$C_{13}H_{10}O_4$ (230.0579)	9			$C_{13}H_{12}O_4$ (232.0736) (No. 6; GUA+DMB POS)		
5	$C_{13}H_{10}O_5$ (246.0528)	9		18	$C_7H_{10}O_5$ (174.0528)	3	
6	$C_{13}H_{12}O_4$ (232.0736)	8		19	$C_{21}H_{18}O_8$ (398.1002)	13	
7	$C_{14}H_{12}O_5$ (260.0685)	9		20	$C_{13}H_{12}O_6$ (264.0634)	8	
8	$C_{11}H_{12}O_5$ (224.0685)	6		21	$C_{20}H_{18}O_6$ (354.1103)	12	
9	$C_{14}H_{12}O_7$ (292.0583)	9		22	$C_{14}H_{14}O_7$ (294.0740)	8	
10	$C_{11}H_{14}O_6$ (242.0790)	5		23	$C_{12}H_{14}O_4$ (222.0892)	6	

11	C$_{18}$H$_{18}$O$_7$ (346.1053)	10		24	C$_{13}$H$_{10}$O$_6$ (262.0477)	9	
12	C$_{10}$H$_{12}$O$_3$ (180.0786)	5		25	C$_{13}$H$_{14}$O$_4$ (234.0892)	7	
13	C$_7$H$_6$O$_4$ (154.0266)	5		26	C$_{14}$H$_{14}$O$_5$ (262.0841)	8	
14	C$_{16}$H$_{18}$O$_6$ (306.1103)	8		C$_{13}$H$_{10}$O$_5$ (246.0528) (No. 5; GUA+DMB POS)			
15	C$_7$H$_6$O$_5$ (170.0215)	5		27	C$_{19}$H$_{16}$O$_6$ (340.0947)	12	
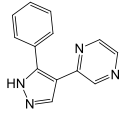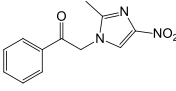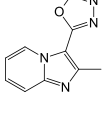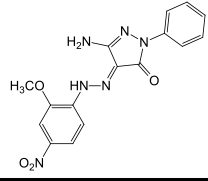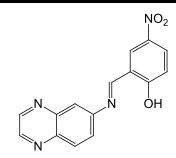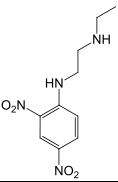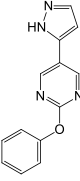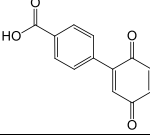
227
228
229
230
231
232
233
234
235
236
237
238
239
240
241
242
243
244
245
246
247
248
249
250
251
252

253 **Table S2**. Possible structures of the major products detected from GUA+VL using UHPLC-
254 HESI- Orbitrap-MS operated in positive (POS) and negative (NEG) ion modes.
255
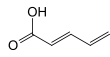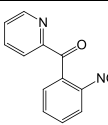
No.	GUA+VL POS Molecular formula and exact mass	DBE	Possible structure	No.	GUA+VL NEG Molecular formula and exact mass	DBE	Possible structure
28	$C_7H_8O_4$ (156.0423)	4		35	$C_8H_8O_5$ (184.0372)	5	
$C_{13}H_{10}O_4$ (230.0579) (No. 4; GUA+DMB, Table S1)				$C_{13}H_{12}O_4$ (232.0736) (No. 6; GUA+DMB, Table S1)			
$C_{13}H_{12}O_4$ (232.0736) (No. 6; GUA+DMB, Table S1)				$C_{14}H_{14}O_4$ (246.0892) (No. 1; GUA+DMB, Table S1)			
$C_{13}H_{10}O_5$ (246.0528) (No. 5; GUA+DMB, Table S1)				$C_{14}H_{14}O_6$ (278.0790) (No. 16; GUA+DMB, Table S1)			
29	$C_7H_8O_5$ (172.0372)	4		$C_{20}H_{18}O_6$ (354.1103) (No. 21; GUA+DMB, Table S1)			
30	$C_6H_6O_2$ (110.0368)	4		$C_{12}H_{10}O_4$ (218.0579) (No. 17; GUA+DMB, Table S1)			
31	$C_{10}H_{10}O_4$ (194.0579)	6		$C_6H_6O_2$ (110.0368) (No. 30; GUA+VL POS)			
32	$C_{11}H_8O_4$ (204.0423)	8		$C_7H_{10}O_5$ (174.0528) (No. 18; GUA+DMB, Table S1)			
33	$C_{12}H_{10}O_3$ (202.0630)	8		36	$C_{15}H_{14}O_5$ (274.0841)	9	
$C_{14}H_{12}O_5$ (260.0685) (No. 7; GUA+DMB, Table S1)				$C_{13}H_{12}O_6$ (264.0634) (No. 20; GUA+DMB, Table S1)			
$C_{13}H_{14}O_4$ (234.0892) (No. 25; GUA+DMB, Table S1)				37	$C_8H_8O_4$ (168.0423)	5	
34	$C_{11}H_{10}O_6$ (238.0477)	7		$C_{19}H_{16}O_6$ (340.0947) (No. 27; GUA+DMB, Table S1)			
$C_{13}H_{10}O_6$ (262.0477) (No. 24; GUA+DMB, Table S1)				$C_{11}H_{10}O_6$ (238.0477) (No. 34; GUA+VL POS)			
$C_{13}H_{12}O_6$ (264.0634) (No. 20; GUA+DMB, Table S1)				38	$C_5H_6O_5$ (146.0215)	3	
$C_7H_6O_4$ (154.0266) (No. 13; GUA+DMB, Table S1)				39	$C_6H_4O_4$ (140.0110)	5	

256

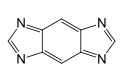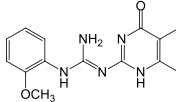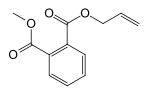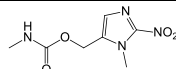| No.	GUA+DMB+AN POS Molecular formula and exact mass	DBE	Possible structure	No.	GUA+DMB +AN NEG Molecular formula and exact mass	DBE	Possible structure
$C_{14}H_{14}O_4$ (246.0892) (No. 1; GUA+DMB, Table S1)				$C_{13}H_{12}O_4$ (232.0736) (No. 6; GUA+DMB, Table S1)			
40	$C_{13}H_{10}N_4$ (222.0905)	11		$C_{14}H_{14}O_6$ (278.0790) (No. 16; GUA+DMB, Table S1)			
$C_{13}H_{10}O_5$ (246.0528) (No. 5; GUA+DMB, Table S1)				$C_{14}H_{14}O_4$ (246.0892) (No. 1; GUA+DMB, Table S1)			
$C_{13}H_{10}O_4$ (230.0579) (No. 4; GUA+DMB, Table S1)				$C_{12}H_{10}O_4$ (218.0579) (No. 17; GUA+DMB, Table S1)			
41	$C_6H_6N_4$ (134.0592)	6		$C_{21}H_{18}O_8$ (398.1002) (No. 19; GUA+DMB, Table S1)			
$C_{13}H_{12}O_4$ (232.0736) (No. 6; GUA+DMB, Table S1)				$C_7H_{10}O_5$ (174.0528) (No. 18; GUA+DMB, Table S1)			
42	$C_{12}H_{11}N_3O_3$ (245.0800)	9		$C_{13}H_{12}O_6$ (264.0634) (No. 20; GUA+DMB, Table S1)			
43	$C_{10}H_8N_4O$ (200.0698)	9		48	$C_{16}H_{14}N_6O_4$ (354.1076)	13	
44	$C_6H_6N_4O$ (150.0542)	6		49	$C_{15}H_{10}N_4O_3$ (294.0753)	13	
45	$C_{10}H_{14}N_4O_4$ (245.1015)	6		$C_{13}H_{10}O_6$ (262.0477) (No. 24; GUA+DMB, Table S1)			
46	$C_{13}H_{10}N_4O$ (238.0855)	11		$C_{10}H_{10}O_4$ (194.0579) (No. 31; GUA+VL, Table S2)			
$C_{13}H_{12}O_6$ (264.0634) (No. 20; GUA+DMB, Table S1)				$C_7H_8O_4$ (156.0423) (No. 28; GUA+VL, Table S2)			
$C_7H_6O_4$ (154.0266) (No. 13; GUA+DMB, Table S1)				$C_{13}H_{14}O_4$ (234.0892) (No. 25; GUA+DMB, Table S1)			
$C_{12}H_{10}O_3$ (202.0630) (No. 33; GUA+VL, Table S2)				$C_{13}H_{10}O_5$ (246.0528) (No. 5; GUA+DMB, Table S1)			
47	$C_{13}H_8O_4$ (228.0423)	10		$C_{14}H_{14}O_5$ (262.0841) (No. 26; GUA+DMB, Table S1)			
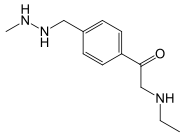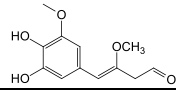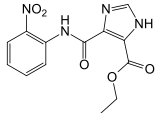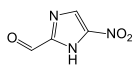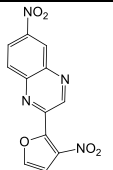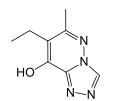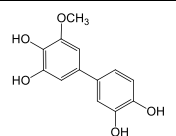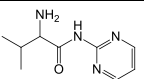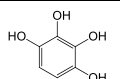
259 **Table S4**. Possible structures of the major products detected from GUA+VL+AN using
260 UHPLC-HESI-Orbitrap-MS operated in positive (POS) and negative (NEG) ion modes.
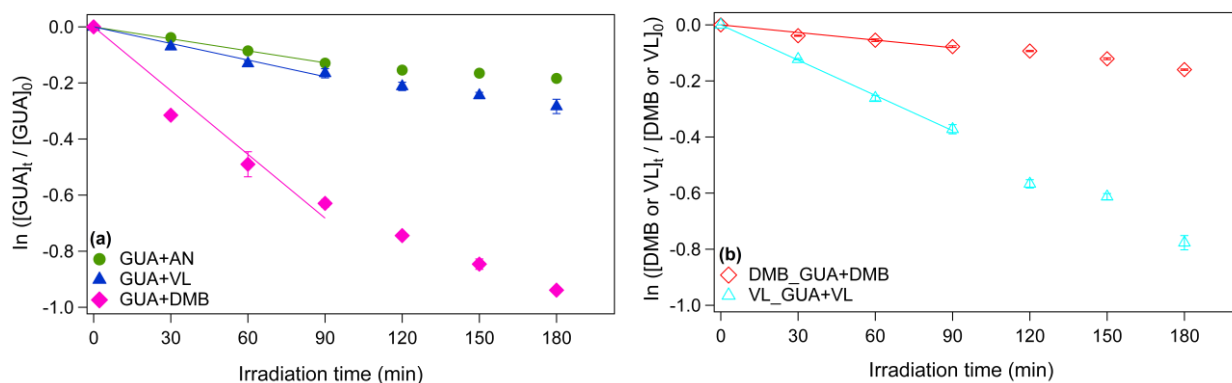261

No.	GUA+VL+AN POS Molecular formula and exact mass	DBE	Possible structure	No.	GUA+VL+AN NEG Molecular formula and exact mass	DBE	Possible structure
	$C_{14}H_{14}O_4$ (246.0892) (No. 1; GUA+DMB, Table S1)				$C_{13}H_{12}O_4$ (232.0736) (No. 6; GUA+DMB, Table S1)		
50	$C_{10}H_8O_2$ (160.0524)	7	(structure)		$C_{14}H_{14}O_6$ (278.0790) (No.16; GUA+DMB, Table S1)		
51	$C_{16}H_{18}O_4$ (274.1205)	8	(structure)		$C_{12}H_{10}O_4$ (218.0579) (No.17; GUA+DMB, Table S1)		
	$C_{11}H_{12}O_5$ (224.0685) (No. 8; GUA+DMB, Table S1)			57	$C_{11}H_9N_3O_3$ (231.0644)	9	(structure)
	$C_{14}H_{12}O_5$ (260.068) (No. 7; GUA+DMB, Table S1)				$C_7H_{10}O_5$ (174.0528) (No.18; GUA+DMB, Table S1)		
	$C_{12}H_{14}O_4$ (222.0892) (No. 23; GUA+DMB, Table S1)				$C_{15}H_{14}O_5$ (274.0841) (No. 36; GUA+VL, Table S2)		
52	$C_{11}H_{12}O_4$ (208.0736)	6	(structure)		$C_{13}H_{12}O_6$ (264.0634) (No. 20; GUA+DMB, Table S1)		
	$C_6H_6N_4O$ (150.0542) (No. 44; GUA+DMB+AN, Table S3)			58	$C_5H_6O_2$ (98.0368)	3	(structure)
	$C_{13}H_{12}O_4$ (232.0736) (No. 6; GUA+DMB, Table S1)				$C_{19}H_{16}O_6$ (340.0947) (No. 27; GUA+DMB, Table S1)		
53	$C_{12}H_8N_2O_3$ (228.0535)	10	(structure)	59	$C_{20}H_{16}O_7$ (368.0896)	13	(structure)
54	$C_{11}H_{14}O_4$ (210.0892)	5	(structure)		$C_{21}H_{18}O_8$ (398.1002) (No. 19; GUA+DMB, Table S1)		
	$C_7H_6O_4$ (154.0266) (No. 13; GUA+DMB, Table S1)				$C_7H_6O_4$ (154.0266) (No. 13; GUA+DMB, Table S1)		
55	$C_{14}H_{12}O_6$ (276.0634)	9	(structure)		$C_{15}H_{10}N_4O_3$ (294.0753) (No. 49; GUA+DMB+AN, Table S3)		
56	$C_{14}H_{10}N_4O_7$ (346.0550)	12	(structure)		$C_{13}H_{10}O_6$ (262.0477) (No. 24; GUA+DMB, Table S1)		
	$C_{13}H_{12}O_6$ (264.0634) (No. 20; GUA+DMB, Table S1)				$C_5H_6O_5$ (146.0215) (No. 38; GUA+VL, Table S2)		

262

Table S5. Possible structures of the major products detected from GUA+AN using UHPLC-
HESI-Orbitrap-MS operated in positive (POS) and negative (NEG) ion modes.

No.	GUA+AN POS Molecular formula and exact mass	DBE	Possible structure	No.	GUA+AN NEG Molecular formula and exact mass	DBE	Possible structure
	$C_{13}H_{10}O_4$ (230.0579) (No. 4; GUA+DMB, Table S1)				$C_{14}H_{14}O_6$ (278.0790) (No. 16; GUA+DMB, Table S1)		
	$C_6H_6N_4O$ (150.0542) (No. 44; GUA+DMB+AN, Table S3)			68	$C_{12}H_{19}N_3O$ (221.1528)	5	
	$C_{11}H_{12}O_5$ (224.0685) (No. 8; GUA+DMB, Table S1)				$C_{12}H_{10}O_4$ (218.0579) (No. 17; GUA+DMB, Table S1)		
	$C_7H_8O_4$ (156.0423) (No. 28; GUA+VL, Table S2)				$C_{14}H_{14}O_4$ (246.0892) (No. 1; GUA+DMB, Table S1)		
60	$C_6H_4N_4$ (132.0436)	7			$C_{20}H_{18}O_6$ (354.1103) (No. 21; GUA+DMB, Table S1)		
61	$C_{12}H_{14}O_5$ (238.0841)	6			$C_7H_{10}O_5$ (174.0528 (No. 18; GUA+DMB, Table S1)		
62	$C_{13}H_{12}N_4O_5$ (304.0808)	10		69	$C_4H_3N_3O_3$ (141.0174)	5	
	$C_{13}H_{12}O_6$ (264.0634) (No. 20; GUA+DMB, Table S1)				$C_{13}H_{12}O_6$ (264.0634) (No. 20; GUA+DMB, Table S1)		
	$C_{13}H_{12}O_4$ (232.0736) (No. 6; GUA+DMB, Table S1)			70	$C_{12}H_6N_4O_5$ (286.0338)	12	
63	$C_8H_{10}N_4O$ (178.0855)	6		71	$C_{13}H_{12}O_5$ (248.0685)	8	
64	$C_9H_{14}N_4O$ (194.1168)	5		72	$C_6H_6O_4$ (142.0266)	4	
65	$C_8H_4N_4$ (156.0436)	9			$C_{12}H_{10}O_3$ (202.0630) (No. 33; GUA+VL, Table S2)		
66	$C_{15}H_{19}N_5O_2$ (301.1539)	9		73	$C_{12}H_{12}O_4$ (220.0736)	7	
67	$C_7H_{10}N_4O_4$ (214.0702)	5			$C_7H_6O_5$ (170.0215) (No. 15; GUA+DMB, Table S1)		
	$C_7H_8O_5$ (172.0372) (No. 29; GUA+VL, Table S2)				$C_7H_8O_4$ (156.0423) (No. 28; GUA+VL, Table S2)		

266

Figure S1. (a) The decay of GUA during (ammonium) nitrate-mediated photo-oxidation (GUA+AN) and photosensitized oxidation by $^3VL^*$ (GUA+VL) or $^3DMB^*$ (GUA+DMB). (b) The decay of DMB or VL during GUA photo-oxidation in GUA+DMB and GUA+VL, respectively. No statistically significant difference ($p > 0.05$) was noted between GUA+DMB and GUA+DMB+AN and between GUA+VL and GUA+VL+AN. Error bars represent 1 standard deviation; most error bars are smaller than the markers.
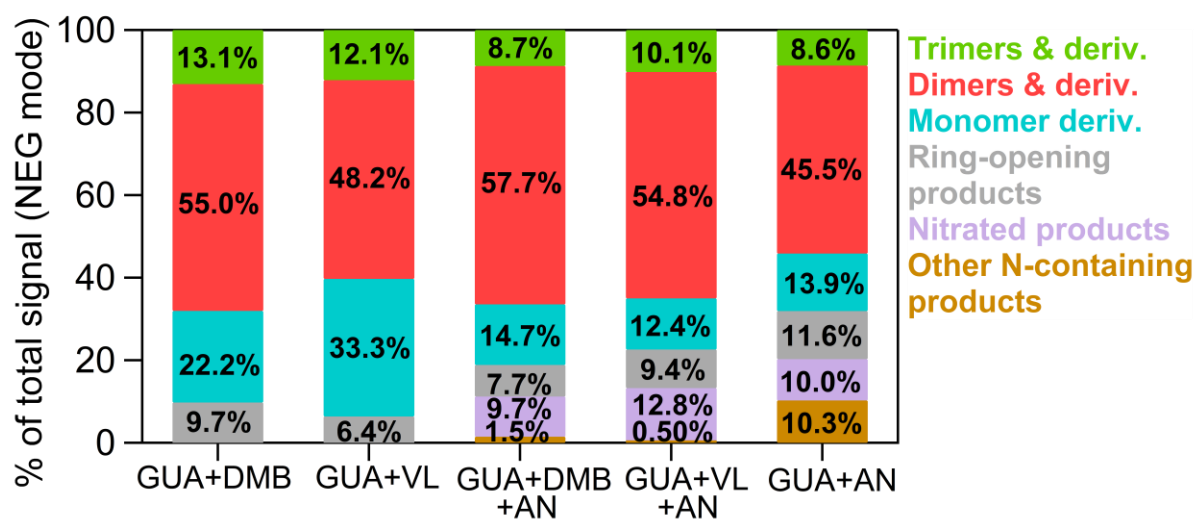
306

307
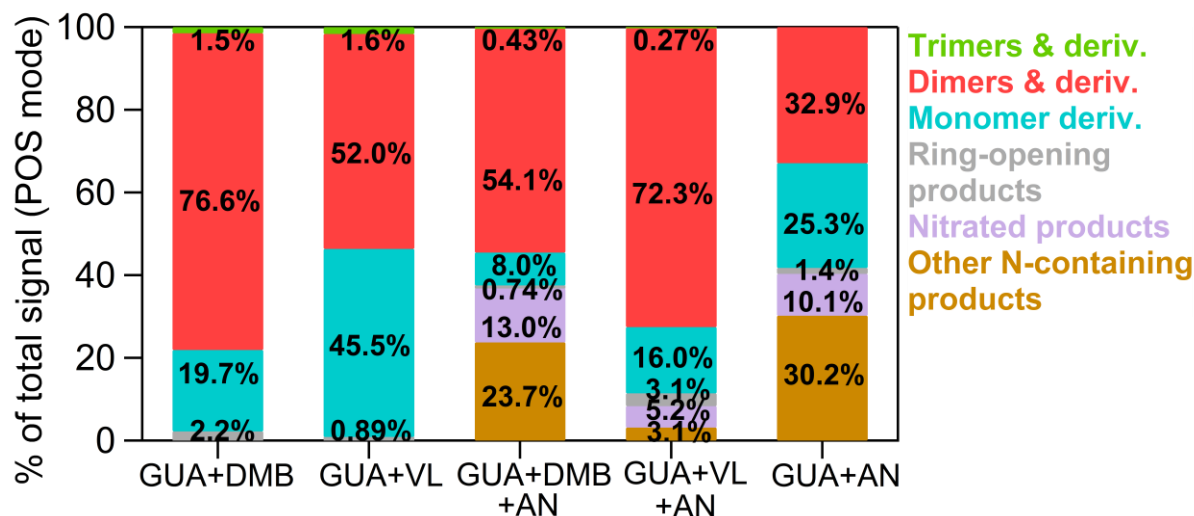
Figure S2~~1~~. Signal-weighted distributions of aqSOA from GUA+DMB, GUA+VL, GUA+DMB+AN, GUA+VL+AN, and GUA+AN. These product distributions were calculated from UHPLC-HESI-Orbitrap-MS data obtained in the positive (POS) ion mode. The values indicate the contribution of different product classifications to the total signals for each reaction condition.

313

Figure S3~~2~~. Signal-weighted distributions of aqSOA from GUA+DMB, GUA+VL, GUA+DMB+AN, GUA+VL+AN, and GUA+AN. These product distributions were calculated from UPLC-HESI-Orbitrap-MS data obtained in the negative (NEG) ion mode. The values indicate the contribution of different product classifications to the total signals for each reaction condition.
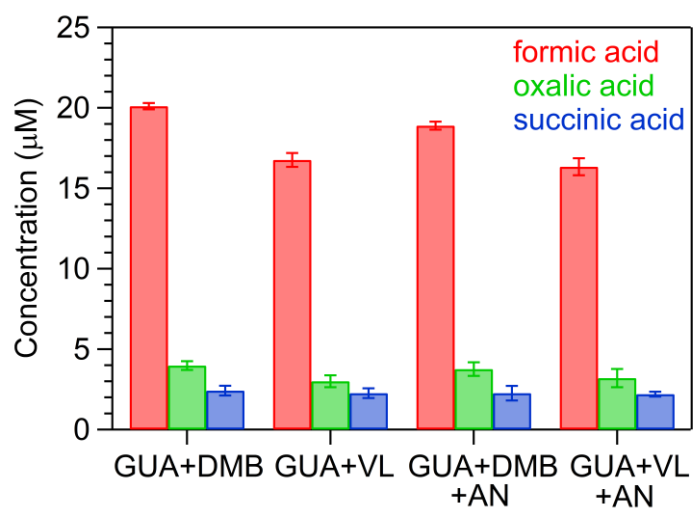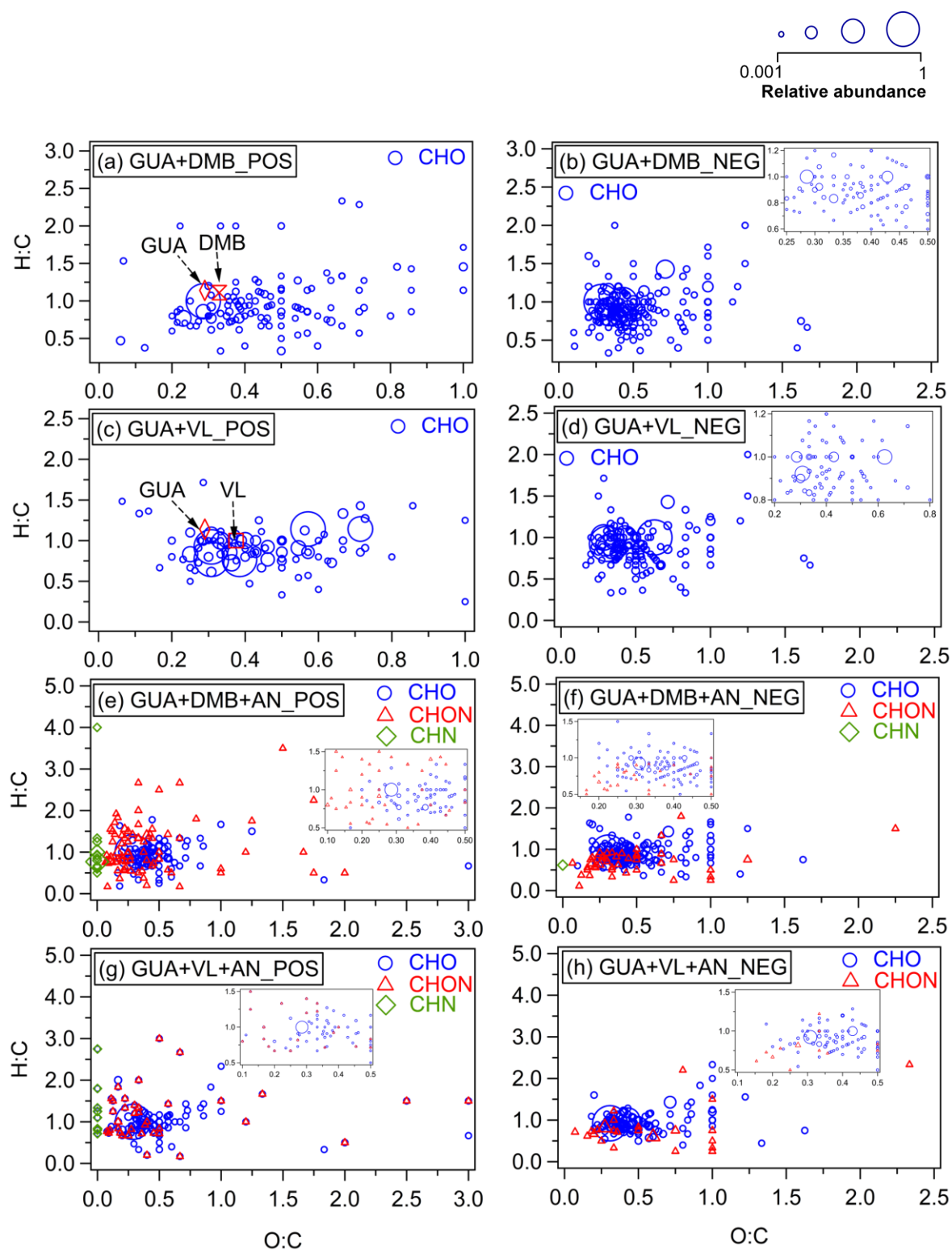
319

320

321

322

323

Figure S43. The concentration of formic, oxalic, and succinic acid for GUA+DMB, GUA+VL, GUA+DMB+AN, and GUA+VL+AN aqSOA. Error bars represent one standard deviation of triplicate experiments.

370

Figure S54. Van Krevelen diagrams of aqSOA from (a, b) GUA+DMB, (c, d) GUA+VL, (e, f) GUA+DMB+AN, and (g, h) GUA+VL+AN for positive (POS) and negative (NEG) ion modes. The blue circle markers indicate CHO classes, red triangle indicate CHON classes, and green diamond indicate CHN classes. The marker size reflects the relative abundance in the sample. The location of GUA, DMB, and VL in the plots are indicated only in panels a and c (red markers). The insets are expanded views of the crowded sections of the van Krevelen diagrams. Note the different scales on the axes.
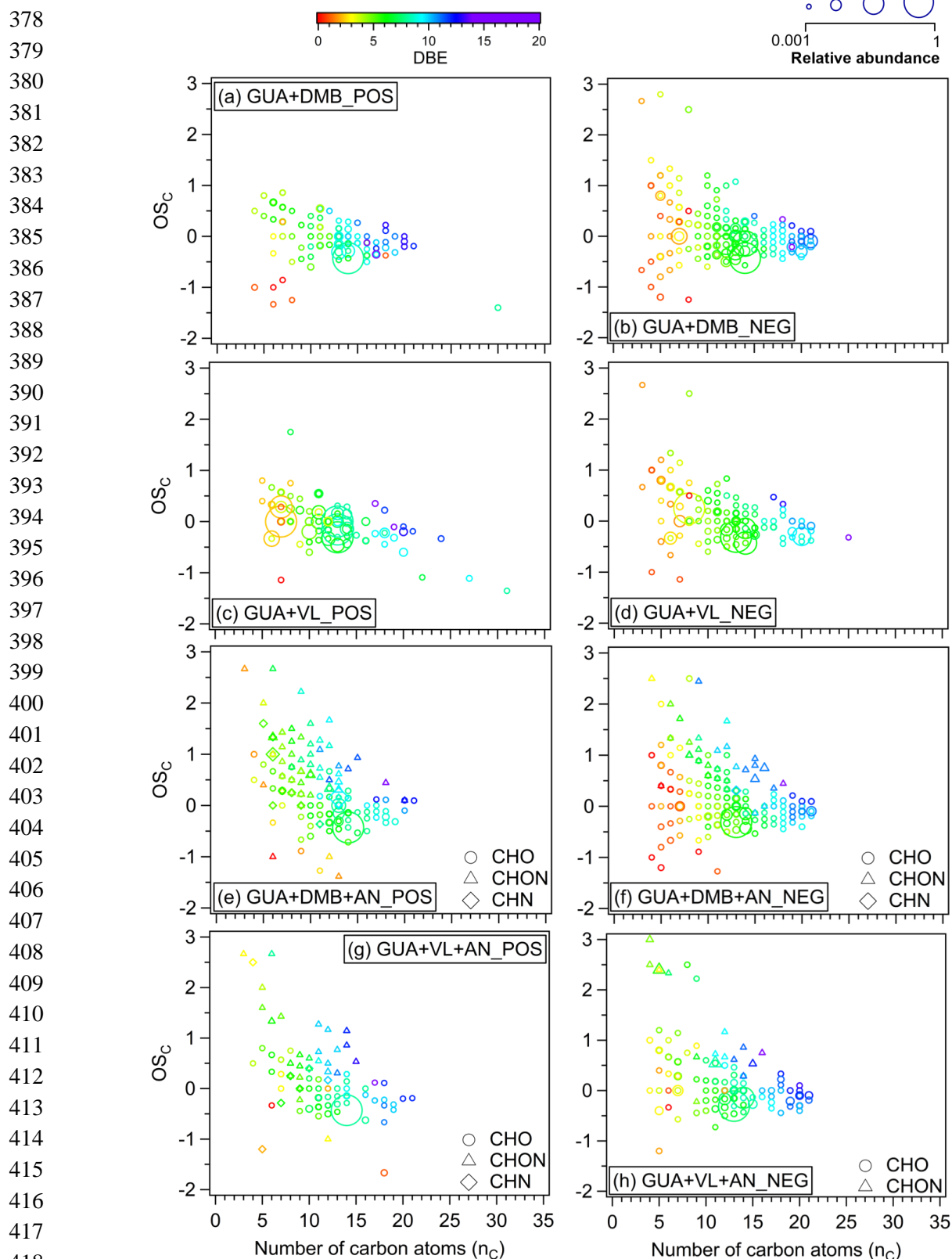
Figure S6. Plots of the carbon oxidation state (OS$_C$) vs. the number of carbon atoms (n$_C$) of aqSOA from (a, b) GUA+DMB, (c, d) GUA+VL, (e, f) GUA+DMB+AN, and (g, h) GUA+VL+AN for positive (POS) and negative (NEG) ion modes, colored by the double bond equivalent (DBE) values. The circle, triangle, and diamond markers indicate CHO, CHON and CHN classes, respectively. The marker size reflects the relative abundance in the sample.

424
425
426
427
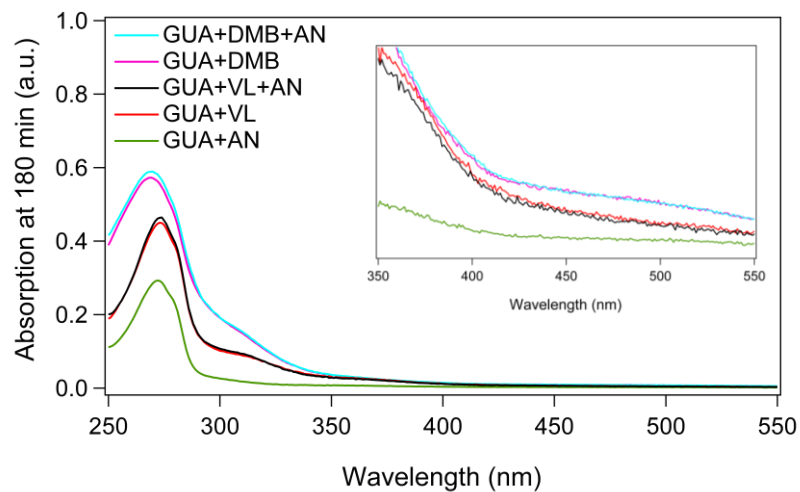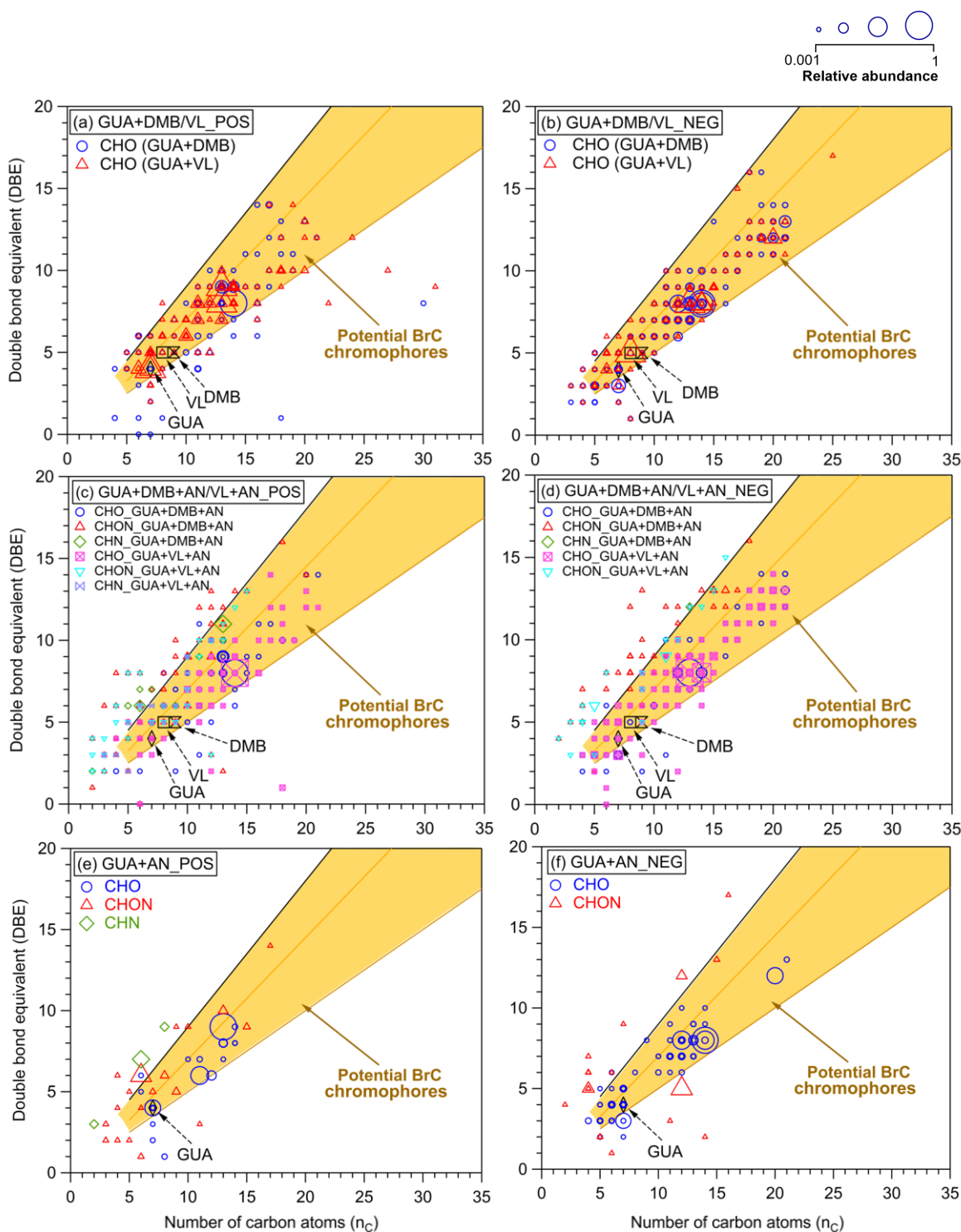428
429
430
431
432
433
434
435
436
437

Figure S7. UV-Vis absorption spectra of GUA+DMB+AN, GUA+DMB, GUA+VL+AN, GUA+VL, and GUA+AN after 180 min of irradiation. The inset is the expanded view from 350 to 550 nm.

442

Figure S86. Plots of the double bond equivalent (DBE) values vs. the number of carbon atoms (nc) (Lin et al., 2018) of aqSOA from (a, b) GUA+DMB and GUA+VL, (c, d) GUA+DMB+AN and GUA+VL+AN, and (e, f) GUA+AN for positive (POS) and negative (NEG) ion modes. For a and b, the blue markers indicate CHO classes for GUA+DMB and red indicate CHO classes for GUA+VL. For c and d, the blue markers indicate CHO classes, red indicate CHON classes, and green indicate CHN classes for GUA+DMB+AN; the pink markers indicate CHO classes, cyan indicate CHON classes, and purple indicate CHN classes for GUA+VL+AN. For e and f, the blue markers indicate CHO classes, red indicate CHON classes, and green indicate

451 CHN classes for GUA+AN. The marker size reflects the relative abundance in the sample. The
452 three lines indicate DBE reference values of fullerene-like hydrocarbons (top, black solid line;
453 Lobodin et al, 2012), cata-condensed polycyclic aromatic hydrocarbons (PAHs; Siegmann and
454 Sattler, 2000) (middle, orange solid line), and linear conjugated polyenes (general formula
455 C_xH_{x+2}) (bottom, brown solid line). Species within the shaded area are potential BrC
456 chromophores.
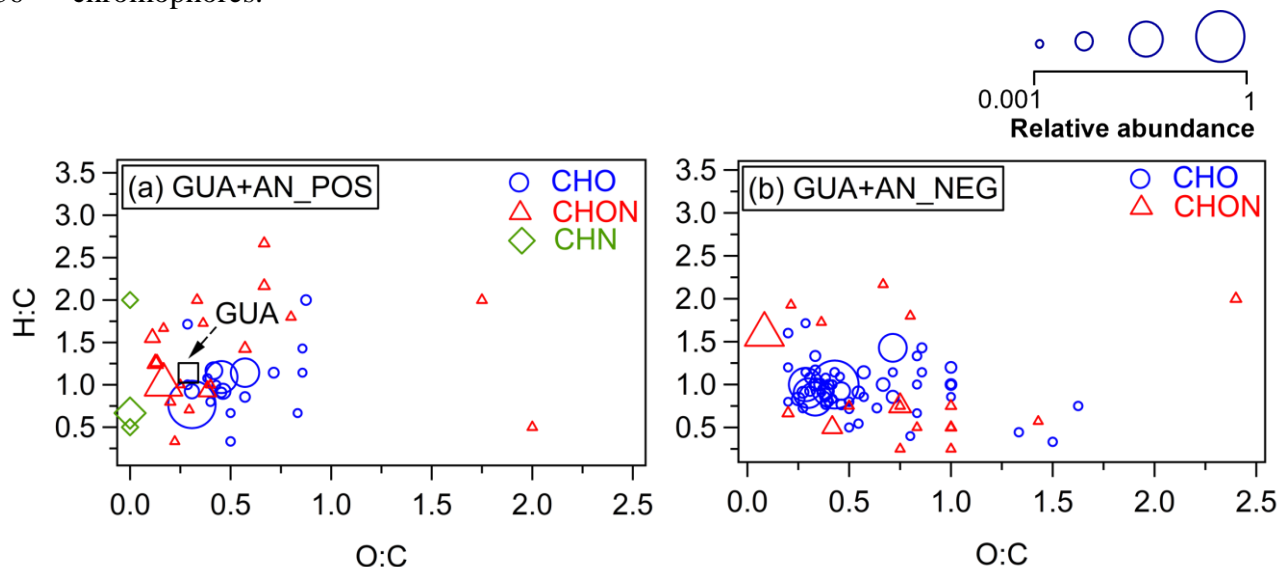
457 **Figure S97.** Van Krevelen diagrams of aqSOA from GUA+AN for (a) positive (POS) and (b)
458 negative (NEG) ion modes. The blue markers indicate CHO classes, red indicate CHON
459 classes, and green indicate CHN classes. The marker size reflects the relative abundance in the
460 sample. The location of GUA is indicated only in panel a (black marker).
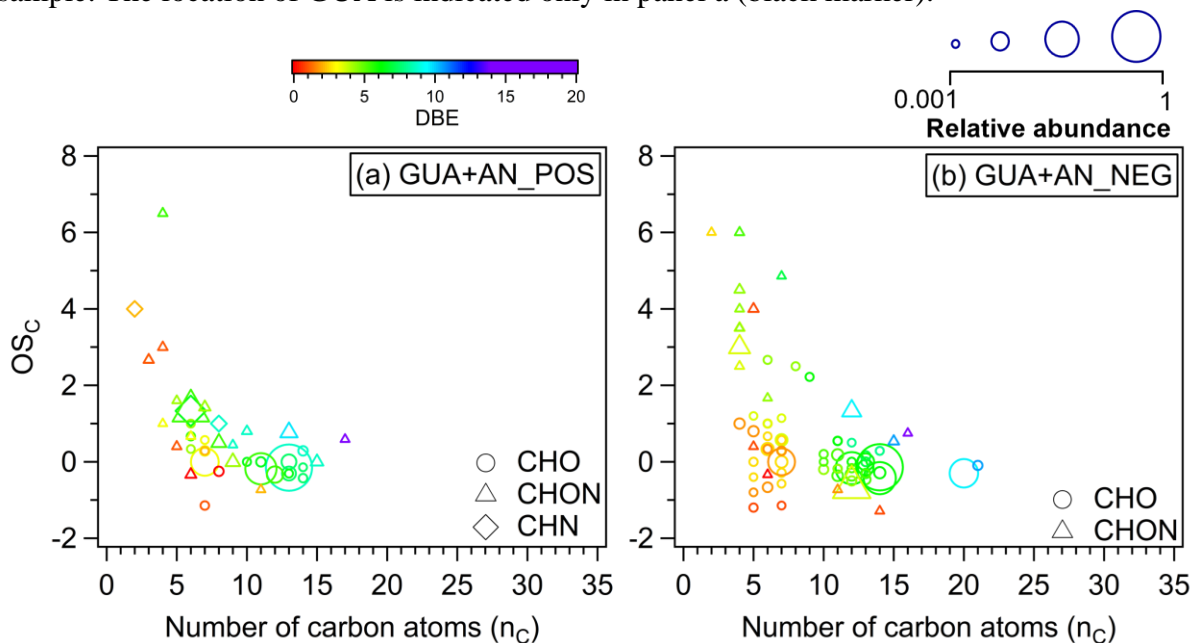
461
462 **Figure S108.** Plots of the carbon oxidation state (OS_C) vs. the number of carbon atoms (n_C) of
463 aqSOA from GUA+AN for (a) positive (POS) and (b) negative (NEG) ion modes, colored by
464 the double bond equivalent (DBE) values. The circle, triangle, and diamond markers indicate
465 CHO, CHON and CHN classes, respectively. The marker size reflects the relative abundance
466 in the sample.

References

Anastasio, C., Faust, B. C., and Rao, C. J.: Aromatic carbonyl compounds as aqueous-phase photochemical sources of hydrogen peroxide in acidic sulfate aerosols, fogs, and clouds. 1. Non-phenolic methoxybenzaldehydes and methoxyacetophenones with reductants (phenols), Environ. Sci. Technol., 31, 218−232, https://doi.org/10.1021/es960359g, 1997.

Bateman, A. P., Laskin, J., Laskin, A., and Nizkorodov, S. A.: Applications of high-resolution electrospray ionization mass spectrometry to measurements of average oxygen to carbon ratios in secondary organic aerosols, Environ. Sci. Technol., 46, 8315–832, https://doi.org/10.1021/es3017254, 2012.

Chen, Y., Li, N., Li, X., Tao, Y., Luo, S., Zhao, Z., Ma, S., Huang, H., Chen, Y., Ye, Z., and Ge, X.: Secondary organic aerosol formation from $^3C^*$-initiated oxidation of 4-ethylguaiacol in atmospheric aqueous-phase, Sci. Total Environ., 723, 137953, https://doi.org/10.1016/j.scitotenv.2020.137953, 2020.

Claeys, M., Vermeylen, R., Yasmeen, F., Gómez-González, Y., Chi, X., Maenhaut, W., Mészáros, T., and Salma, I.: Chemical characterization of humic-like substances from urban, rural and tropical biomass burning environments using liquid chromatography with UV/vis photodiode array detection and electrospray ionization mass spectrometry, Environ. Chem., 9, 273–284, https://doi.org/10.1071/EN11163, 2012.

He, L., Schaefer, T., Otto, T., Kroflič, A., and Herrmann, H.: Kinetic and theoretical study of the atmospheric aqueous-phase reactions of OH radicals with methoxyphenolic compounds, J. Phys. Chem. A, 123, 7828−7838, https://doi.org/10.1021/acs.jpca.9b05696, 2019.

Jiang, W., Misovich, M. V., Hettiyadura, A. P. S., Laskin, A., McFall, A. S., Anastasio, C., and Zhang, Q.: Photosensitized reactions of a phenolic carbonyl from wood combustion in the aqueous phase—chemical evolution and light absorption properties of aqSOA, Environ. Sci. Technol., 55, 5199−5211, https://doi.org/10.1021/acs.est.0c07581, 2021.

Koch, B. P. and Dittmar, T.: From mass to structure: an aromaticity index for high-resolution mass data of natural organic matter, Rapid Commun. Mass Spectrom., 20, 926–932, https://doi.org/10.1002/rcm.2386, 2006.

Kourtchev, I., Godoi, R. H. M., Connors, S., Levine, J. G., Archibald, A. T., Godoi, A. F. L., Paralovo, S. L., Barbosa, C. G. G., Souza, R. A. F., Manzi, A. O., Seco, R., Sjostedt, S., Park, J., Guenther, A., Kim, S., Smith, J., Martin, S. T., and Kalberer, M.: Molecular composition of organic aerosols in central Amazonia: an ultra-high-resolution mass spectrometry study, Atmos. Chem. Phys., 16, 11899–11913, https://doi.org/10.5194/acp-16-11899-2016, 2016.

Kroll, J. H., Donahue, N. M., Jimenez, J. L., Kessler, S. H., Canagaratna, M. R., Wilson, K. R., Altieri, K. E., Mazzoleni, L. R., Wozniak, A. S., Bluhm, H., Mysak, E. R., Smith, J. D., Kolb, C. E., and Worsnop, D. R.: Carbon oxidation state as a metric for describing the chemistry of atmospheric organic aerosol, Nat. Chem., 3, 133–139, https://doi.org/10.1038/nchem.948, 2011.

Kroll, J. H., Lim, C. Y., Kessler, S. H., and Wilson, K. R.: Heterogeneous oxidation of atmospheric organic aerosol: kinetics of changes to the amount and oxidation state of particle-

517 phase organic carbon, J. Phys. Chem. A, 119, 10767−10783,
518 https://doi.org/10.1021/acs.jpca.5b06946, 2015.

520 Laskin, J., Laskin, A., Nizkorodov, S. A., Roach, P., Eckert, P., Gilles, M. K., Wang, B., Lee,
521 H. J., and Hu, Q.: Molecular selectivity of brown carbon chromophores, Environ. Sci. Technol.,
522 48, 12047–12055, https://doi.org/10.1021/es503432r, 2014.

524 Li, Y. J., Huang, D. D., Cheung, H. Y., Lee, A. K. Y., and Chan, C. K.: Aqueous-phase
525 photochemical oxidation and direct photolysis of vanillin - a model compound of methoxy
526 phenols from biomass burning, Atmos. Chem. Phys., 14, 2871−2885,
527 https://doi.org/10.5194/acp-14-2871-2014, 2014.

529 Lin, P., Fleming, L. T., Nizkorodov, S. A., Laskin, J., and Laskin, A.: Comprehensive
530 molecular characterization of atmospheric brown carbon by high resolution mass spectrometry
531 with electrospray and atmospheric pressure photoionization, Anal. Chem., 90, 12493–12502,
532 https://doi.org/10.1021/acs.analchem.8b02177, 2018.

534 Lobodin, V. V., Marshall, A. G., and Hsu, C. S.: Compositional space boundaries for organic
535 compounds, Anal. Chem., 84, 3410–3416, https://doi.org/10.1021/ac300244f, 2012.

537 Lv, J., Zhang, S., Luo, L., and Cao, D.: Solid-phase extraction-stepwise elution (SPE-SE)
538 procedure for isolation of dissolved organic matter prior to ESI-FT-ICR-MS analysis, Anal.
539 Chim. Acta, 948, 55−61, https://doi.org/10.1016/j.aca.2016.10.038, 2016.

541 Mabato, B. R. G., Lyu, Y., Ji, Y., Li, Y. J., Huang, D. D., Li, X., Nah, T., Lam, C. H., and
542 Chan, C. K.: Aqueous secondary organic aerosol formation from the direct photosensitized
543 oxidation of vanillin in the absence and presence of ammonium nitrate, Atmos. Chem. Phys.,
544 22, 273−293, https://doi.org/10.5194/acp-22-273-2022, 2022.

546 Misovich, M. V., Hettiyadura, A. P. S., Jiang, W., Zhang, Q., and Laskin, A.: Molecular-level
547 study of the photo-oxidation of aqueous-phase guaiacyl acetone in the presence of ^{3}C*:
548 formation of brown carbon products, ACS Earth Space Chem., 5, 1983−1996,
549 https://doi.org/10.1021/acsearthspacechem.1c00103, 2021.

551 Schmitt-Kopplin, P., Gelencsér, A., Dabek-Zlotorzynska, E., Kiss, G., Hertkorn, N., Harir, M.,
552 Hong, Y., and Gebefügi, I.: Analysis of the unresolved organic fraction in atmospheric aerosols
553 with ultrahigh–resolution mass spectrometry and nuclear magnetic resonance spectroscopy:
554 organosulfates as photochemical smog constituents, Anal. Chem., 82, 8017–8026,
555 https://doi.org/10.1021/ac101444r, 2010.

557 Siegmann, K. and Sattler, K.: Formation mechanism for polycyclic aromatic hydrocarbons in
558 methane flames, J. Chem. Phys., 112, 698–709, https://doi.org/10.1063/1.480648, 2000.

560 Smith, J. D., Sio, V., Yu, L., Zhang, Q., and Anastasio, C.: Secondary organic aerosol
561 production from aqueous reactions of atmospheric phenols with an organic triplet excited state,
562 Environ. Sci. Technol., 48, 1049–1057, https://doi.org/10.1021/es4045715, 2014.

564 Smith, J. D., Kinney, H., and Anastasio, C.: Phenolic carbonyls undergo rapid aqueous
565 photodegradation to form low-volatility, light-absorbing products, Atmos. Environ., 126,
566 36−44, https://doi.org/10.1016/j.atmosenv.2015.11.035, 2016.

567   Yee, L. D., Kautzman, K. E., Loza, C. L., Schilling, K. A., Coggon, M. M., Chhabra, P. S.,
568   Chan, M. N., Chan, A. W. H., Hersey, S. P., Crounse, J. D., Wennberg, P. O., Flagan, R. C.,
569   and Seinfeld, J. H.: Secondary organic aerosol formation from biomass burning intermediates:
570   phenol and methoxyphenols, Atmos. Chem. Phys., 13, 8019–8043,
571   https://doi.org/10.5194/acp- 13-8019-2013, 2013.
572

573   Yu, L., Smith, J., Laskin, A., Anastasio, C., Laskin, J., and Zhang, Q.: Chemical
574   characterization of SOA formed from aqueous-phase reactions of phenols with the triplet
575   excited state of carbonyl and hydroxyl radical, Atmos. Chem. Phys., 14, 13801−13816,
576   https://doi.org/10.5194/acp-14-13801-2014, 2014.
577

578   Yu, L., Smith, J., Laskin, A., George, K. M., Anastasio, C., Laskin, J., Dillner, A. M., and
579   Zhang, Q.: Molecular transformations of phenolic SOA during photochemical aging in the
580   aqueous phase: competition among oligomerization, functionalization, and fragmentation,
581   Atmos. Chem. Phys., 16, 4511−4527, https://doi.org/10.5194/acp-16-4511-2016.